

See discussions, stats, and author profiles for this publication at: <https://www.researchgate.net/publication/275723803>

SHIA_Landslide: a distributed conceptual and physically based model to forecast the temporal and spatial occurrence of shallow landslides triggered by rainfall in tropical and moun...

Article in *Landslides* · April 2015

DOI: 10.1007/s10346-015-0580-7

CITATIONS

57

4 authors:



Edier Aristizábal
Universität Potsdam
86 PUBLICATIONS 673 CITATIONS

[SEE PROFILE](#)

READS

1,225



Jaime Ignacio Velez
National University of Colombia
85 PUBLICATIONS 838 CITATIONS

[SEE PROFILE](#)



Hernán Eduardo Martínez
Integral S.A. Ingenieros Consultores
84 PUBLICATIONS 562 CITATIONS

[SEE PROFILE](#)



Michel Jaboyedoff
University of Lausanne
638 PUBLICATIONS 12,070 CITATIONS

[SEE PROFILE](#)

Some of the authors of this publication are also working on these related projects:



Turtle Mountain Monitoring Project [View project](#)



Programa de Investigación de la gestión integral del agua (GRECIA): Manejo integral de microcuencas costeras. [View project](#)

SHIA_Landslide: a distributed conceptual and physically based model to forecast the temporal and spatial occurrence of shallow landslides triggered by rainfall in tropical and mountainous basins

Abstract Landslides are a main cause of human and economic losses worldwide. For this reason, landslide hazard assessment and the capacity to predict this phenomenon have been topics of great interest within the scientific community for the implementation of early warning systems. Although several models have been proposed to forecast shallow landslides triggered by rainfall, few models have incorporated geotechnical factors into a complete hydrological model of a basin that can simulate the storage and movement of rainwater through the soil profile. These basin and full hydrological models have adopted a physically based approach. This paper develops a conceptual and physically based model called open and distributed hydrological simulation and landslides—SHIA_Landslide (*Simulación Hidrológica Abierta*, or SHIA, in Spanish)—that is supported by geotechnical and hydrological features occurring on a basin-wide scale in tropical and mountainous terrains. SHIA_Landslide is an original and significant contribution that offers a new perspective with which to analyse shallow landslide processes by incorporating a comprehensive distributed hydrological tank model that includes water storage in the soil coupled with a classical analysis of infinite slope stability under saturated conditions. SHIA_Landslide can be distinguished by the following: (i) its capacity to capture surface topography and effects concerning the subsurface flow; (ii) its use of digital terrain model (DTM) to establish the relationships among cells, geomorphological parameters, slope angle, direction, etc.; (iii) its continuous simulation of rainfall data over long periods and event simulations of specific storms; (iv) its consideration of the effects of horizontal and vertical flow; and (vi) its inclusion of a hydrologically complete water process that allows for hydrological calibration. SHIA_Landslide can be combined with real-time rainfall data and implemented in early warning systems.

Keywords Landslides · Rainfall · Physical model · Tropical environments

Introduction

Landslides are one of the main causes of global human and economic losses (Schuster 1996; Sidle and Ochiai 2006). Vulnerability to landslide hazards has increased due to expanded land urbanisation in areas with high landslide susceptibility. Therefore, landslide hazard assessment and the capacity to predict such phenomena have been a topic of great interest within the scientific community, with the goal of implementing early warning systems (Aleotti and Chowdhury 1999; Chacón et al. 2006; Godt et al. 2012; Cepeda et al. 2010; NOAA-USGS 2005; Restrepo et al. 2008; Larsen 2008).

In terms of the issue on landslide magnitude, numerous studies have been conducted in recent years that have helped increase

understanding of the causes involved in these morphodynamic processes. However, due to the complexity of landslide events, there is still great uncertainty when predicting their occurrence. Landslides are caused by a variety of hydrological, geological and anthropological factors, compelling researchers to take an interdisciplinary approach to predicting their occurrence (Crosta and Frattini 2008). The factors controlling the occurrence and distribution of landslides can be categorised as quasi-static variables or dynamic variables. The quasi-static variables, such as soil properties and topography, contribute to slope susceptibility, which defines the spatial distribution of landslides. Dynamic variables, such as rainfall and earthquakes, control the triggering factors on landslide-prone slopes and characterise landslides' temporal patterns (Brunsden 2002; Crosta and Frattini 2003).

Shallow landslides triggered by rainfall, usually called soil slips, have a planar slip surface. These landslides are characterised by their shallow thicknesses (0.3–2 m), which are much smaller than their flow lengths, and by the slip of the surface fault parallel to the slope and the escarpment's small area (Anderson and Sitar 1995). Two different failure mechanisms induced by rainfall have been discussed in the literature. The first mechanism is based on the idea of increasing the density and reducing the hydraulic conductivity of the weathering profile with increasing depth (Terlien 1998; Crosta 1998; Crosta and Frattini 2003; Collins and Znidarcic 2004). In this case, the rainfall rate exceeds the percolation rate, creating a perched subsurface water flow in the residual soil parallel to the slope. Failure occurs due to increased pore pressure caused by the rapid reduction of shear strength in undrained conditions, which has been called static liquefaction of the material by several authors (Hutchinson and Bhandari 1971; Anderson and Sitar 1995; Take et al. 2004; Sassa and Wang 2005; Askarinejad et al. 2012). The second failure mechanism proposes the development of an advancing wetting front from the slope surface in which the material is still in an unsaturated state when failure occurs due to reduced suction, as the mass behaves like a rigid body (Rahardjo et al. 1995; Wang and Sassa 2003; Collins and Znidarcic 2004).

The complexity of calculating the probability of obtaining an increased critical pore pressure or reduced suction and, consequently, predicting a rainfall-triggered landslide occurrence is a function of many intimately related parameters. One of the most important recent advances that have allowed researchers to consider all of these variations is the use of physical and hydrological distributed models (Wu and Sidle 1995; Borga et al. 1998; Crosta 1998; Burton and Bathurst 1998; Griffiths and Collison 1999; Frattini et al. 2004; Vélez et al. 2004).

Physically based models propose hillside hydrology as a subsurface flow in a steady-state (Montgomery and Dietrich 1994) or vertical transient dynamic flows, assessing the landslide hazard for specific storms (Iverson 2000). Other models based on the static

state in kinematic wave hydrology have been used for saturated hillside slopes in many studies (Troch et al. 2002; Paniconi et al. 2003; Rezzoug et al. 2005). However, the water pressure head within a weathering profile is the sum of two components, the initial steady-state pressure head produced by a long-term average infiltration rate and the transient pressure head response in the short term caused by a given rainstorm (Iverson 2000; D'Odorico et al. 2005).

Several models are available in the literature. One of the first and most recognised physical models has been proposed by Montgomery and Dietrich (1994) and is called SHALSTAB. This model employs a TOPOG hydrological model (O'Loughlin 1986) to estimate the saturated profile height portion, and the method assumes that the dominant control of landslides' spatial distribution is given by topography where the defined slope angles and subsurface flows converge. The Stability Index MAPping (SINMAP), developed by Pack et al. (1998), and the Level I Stability Analysis (LISA), developed by Hammond et al. (1992), are similar models using this approach.

Wu and Sidle (1995) have developed the distributed Shallow Landslide Model (dSLAM), modified as the Integrated Dynamic Slope Stability Model (IDSSM) by Dhakal and Sidle (2003), which is a dynamic and distributed physical model of stability combined with a continuous dynamic vegetation root strength approach. The model uses an infinite slope stability analysis with a slope-parallel subsurface and saturated surface kinematic wave modelling approach proposed by Takasao and Shiiba (1988).

CHASM, the Combined Hydrological And Stability Model, is a distributed physically based two-dimensional model developed by Anderson and Lloyd (1991). The hydrological module simulates flow between adjacent cells in one dimension using the Darcy equation for saturated flow and simulates a vertical flow using the Richards equation for unsaturated conditions. The geotechnical module evaluates slope stability using Bishop's simplified circular method (Bishop 1955).

Baum et al. (2002) have developed a Fortran program called TRIGRS based on the transient one-dimensional vertical infiltration model created by Iverson (2000). The model proposes to evaluate slope stability during a rainfall event as a function of depth and time, reflecting the response of pore pressure. In addition, the model divides the factor of safety into a static component and a component that varies with time. Rossi et al. (2013) have proposed a similar approach called High REsolution Slope Stability Simulator (HIRESSS) using the analytical approximate solution of the Richards equation. The model is inserted into a Monte Carlo simulation to overcome the input parameters' uncertainty issues.

Simoni et al. (2008) have proposed a model for the simulation of rainfall-induced shallow landslides called GEOtop-FS. The model combines infinite slope stability analysis with a spatially distributed finite difference hydrological model and the hydrological model GEOtop (Bertoldi and Rigan 2004) using a probabilistic approach. GEOtop simulates the moisture content and pore pressure evolution resulting from infiltration and models subsurface saturated and unsaturated flows, surface runoff, and channel flows by solving the Richards equation in a three-dimensional physical environment.

Apip et al. (2010) have developed a one-dimensional, integrated, distributed and physically based hydrological and slope

stability modelling system as a tool for predicting land surface susceptibility to landslides at the catchment scale. The model uses a kinematic wave rainfall-runoff to predict the dynamics of soil saturation in each grid element (Kojima and Takara 2003) and simulates three lateral flow mechanisms: subsurface flow through capillary pores, subsurface flow through noncapillary pores and surface flow on the soil layer. Two outputs are produced as follows: (i) a map of the time-invariant spatial distribution of areas susceptible to slope instability and (ii) a map linked with spatiotemporally varying hydrological properties to create a time-varying estimate of susceptibility to slope movement in response to rainfall.

Arnone et al. (2011) have implemented an infinite slope and movement module in a physically based, distributed hydrological model, called TIN-based Real-Time Integrated Basin Simulator (tRIBS), developed by Ivanov et al. (2004). The hydrological model includes physical representations of rainfall interception, evapotranspiration, infiltration with continuous soil moisture accounting, lateral moisture transfer in the unsaturated and saturated zones and runoff routing. The soil movement module assesses possible post-failure movement using an empirical approach where landslides move unconditionally on slopes greater than a critical threshold (Burton and Bathurst 1998).

Until now, the available models have been applied to very specific environmental conditions that do not allow for adjustment to particular rainfall and terrain complexities, such as those for tropical and mountainous terrains. This study developed a conceptual and physically based model called SHIA_Landslide for the prediction of rainfall-triggered shallow landslides in tropical environments and complex terrains. The model is based on the open and distributed hydrological simulation methodology developed by Vélez (2001). SHIA_Landslide is an original and significant contribution that offers a new perspective with which to analyse shallow landslide processes by incorporating a comprehensive distributed hydrological tank model that includes water storage in the soil and a geotechnical, classical analysis of infinite slope stability under saturated conditions. This research was conducted to improve understanding of the mechanisms associated with slope instability and rainfall infiltration in mountainous areas located in rainy environments, where increased population pressure has led to the expansion of development into landslide-prone areas.

Theoretical aspects of the SHIA_Landslide

SHIA_Landslide is supported by geotechnical and hydrological features occurring over a wide basin scale. The model simulates hydrological responses on a regular grid mesh simulating all the main components of the hydrological cycle. A slope stability analysis is performed for each computational element according to the soil water content using an infinite limit equilibrium stability module. The following sections introduce the SHIA_Landslide model and present a case study.

Mechanism of shallow landslides triggered by rainfall in tropical environments

Rainfall is a common phenomenon in tropical climate conditions and results in deep weathering profiles under saturated or near saturated conditions. These events are characterised by a wide

range of physical and mechanical properties that control rainfall infiltration and subsurface flow formation.

Based on studies by Little (1969), Deere and Patton (1971) and Anon (1995), the tropical residual soil profile can be simplified into three basic types of particular qualities to which engineering characteristics are assigned (Fig. 1). (i) Residual soil material is converted to soil and mass structures, and fabric material is decomposed, with significant changes in volume that increase permeability and hydraulic conductivity. This upper soil horizon is influenced by the vegetation root zone, animal disturbances and chemical processes, generating macropore structures such as natural soil pipes or open relict joints. These structures develop a secondary porosity system, substantially increasing the permeability of soils acting as preferential flow paths for subsurface flows. The secondary pores allow for a rapid increase in saturation, and water pore pressure builds up. (ii) Saprolite's mass properties are still 'soil-like' and range from highly to completely weathered material, where the original structures and fabric are preserved by the pseudomorphous replacement of clay minerals and a lack of subsequent disturbance or transportation. Lastly, (iii) slightly weathered to fresh rock has dominating rock-like characteristics and very low permeability.

In terms of the soil's water content, its storage capacity depends on the open spaces or pores found within the soil (Fig. 2). When water falls on a land surface during precipitation, some water filters into the ground, filling voids among the soil particles. While the pull of gravity tends to draw water downward, soils in unsaturated conditions are able to hold some water within their smaller voids due to surface tension forces (Fredlund and Rahardjo 1993). This water is called capillary water. If gravity exerts a force sufficient to exceed surface tension, the excess water will flow downward. This water is called gravitational water, and the water content boundary in the soil is called the field capacity (W_{fc}). W_{fc} is reached when the soil suction is approximately 30 kPa in clay or loam soils or 10 kPa in sandy soils (Richards and Weaver 1944; Saxton and Rawls 2006). Excess water over the field capacity drains freely, according to the soil permeability, until the field capacity point is reached again. The water content below the field capacity point is removed by evapotranspiration until the permanent wilting point (W_{pwp}) is reached. At this point, the volumetric water content is too low for the plant to remove water from the soil, which corresponds to 1,500 kPa of soil suction (Veihmeyer and Hendrickson 1928; Saxton and Rawls 2006).

In this regard, shallow landslides occur due to increasing pore pressure. A weathering soil profile increases the soil's density with depth and a corresponding decrease in hydraulic conductivity. When the rainfall rate exceeds the percolation rate between the residual soil and saprolite, a saturated water flow phenomenon parallel to the slope inclination, known as subsurface flow, starts to form. This means that the potential failure surface is located at or near the level of contact between the relatively permeable residual soil and the underlying, relatively impermeable saprolite. The results of such shallow landslides occur in the form of liquefied soil masses, such as soil slips or mud/debris, due to the rapid reduction of shear strength in undrained conditions, in which the displaced landslide material changes suddenly into a flow (Hutchinson and Bhandari 1971; Anderson and Sitar 1995; Sassa and Wang 2005). Regarding the water content of the soil, for assigned slope value and friction angle, unsaturated conditions dominate during the initial rainfall period

controlling soil mechanics, and shallow landslides may occur through suction reduction when the rainfall accumulated over previous days has been very low. However, after a short period of rainfall, saturated conditions appear and control the occurrence of shallow landslides.

Considering this slope failure mechanism, the shallow landslides triggered by rainfall in tropical environments are controlled by the weathering tropical profile and the soil's water storage capacity. Although the simulation required simplifying both elements into their hydrological and geotechnical components, assumptions had to be carefully weighed and factors playing main roles noted.

Hydrological analysis

The hydrological module implemented to develop the model is formed by two fundamental components: a water balance that simulates the dominant hydrological processes in the catchment and a routing component that simulates the flow of water through the river network. Initially, the overland, subsurface and base flows are defined by a 3-dimensional mesh of connected tanks that drain towards the corresponding tank into the downstream cell, following the surface flow directions until it reaches the channel network. A more detailed description of the SHIA can be found in Vélez (2001), Vélez et al. (2004) and Frances et al. (2007). Regarding the computational program, the catchment is divided into regular horizontally layered grid cells to control the vertical and horizontal connections and flows (Fig. 3).

The vertical connections between tanks describe the rainfall, evapotranspiration, infiltration and percolation processes. Based on the tropical weathering profile, each grid cell is formed by three soil horizons with three different saturated hydraulic conductivities: residual soil (K_s), saprolite (K_p) and rock (K_{pp}), where the residual soil is more permeable than the underlying saprolite soil and the impermeable rock.

The horizontal connections describe the overland flow, subsurface flow and base flow. The model considers the horizontal transfer of water to eight possible neighbouring cells separated by 45° by using a single flow direction submodel. Horizontal connections are based on the topology of the basin built on a grid cell type. There are three types of grid cells: (i) slopes, (ii) rill or ephemeral channels and (iii) perennial channels. The type of grid cell is a function of the drainage area, making it necessary to establish two drainage area thresholds, slopes-rill and rill-perennial channels, both of which must be defined by considering fieldwork observation and local studies.

Each grid cell corresponds to a system of five interconnected tanks that communicate with their respective tank in the downstream cell (Fig. 3). This system represents the water flow and storage as a hydrological response unit. The first four tanks represent the basin's runoff production processes, while the last tank represents the transfer process runoff. Further descriptions are provided below.

The *first tank* (T_1) is called *static storage* and represents interception and water detention in puddles and the capillary water storage in the soil rooting zone, which is a function of field capacity and effective root depth. The amount of water that enters the static storage (D_s) during a time step is the minimum value (Min) between a function of the static storage content and the available volume of T_1 . To estimate the amount of rainfall that

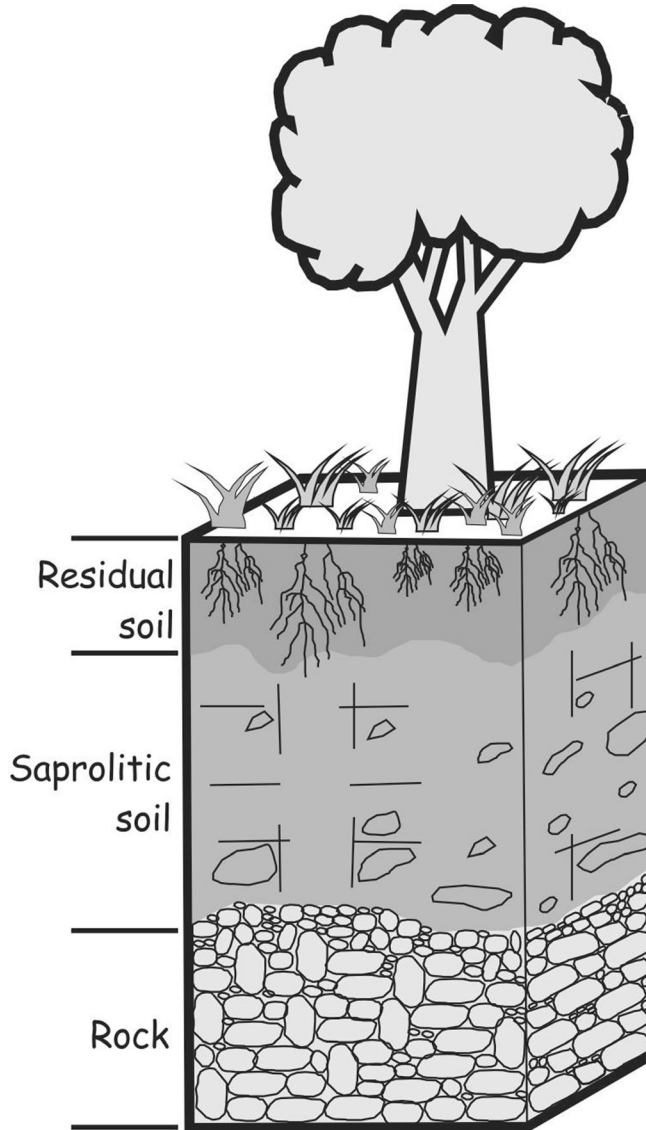


Fig. 1 Typical weathering profile of tropical environments and complex terrains

enters the static storage, several hydrological models use a ratio of water content to maximum capacity with an exponent value between 1 and 3, including the HBV model (Bergström 1995) and GR-3H (Arnaud and Lavabre 1995). Vélez (2001) has proposed an exponent of 2 for tropical environments.

$$D_1 \langle \text{mm} \rangle = \text{Min} \left\{ R_i \left[1 - \left(\frac{S_1^{t-\Delta t}}{S_{1\max}} \right)^2 \right], S_{1\max} - S_1^{t-\Delta t} \right\} \quad (1)$$

where R_i is the rainfall, $S_{1\max}$ is the maximum capacity of T1 and $S_1^{t-\Delta t}$ is the final volume of water in the previous time step in T1. When the volume of water in T1 increases, the volume of water capable of entering T1 decreases. The maximum volume of water that could enter T1 is available when the tank is empty.

The maximum capacity of T1 is

$$S_{1\max} \langle \text{mm} \rangle = (W_{fc} - W_{pwp}) Z_r \quad (2)$$

where W_{fc} is the volumetric soil moisture content remaining at field capacity and W_{pwp} is that at the permanent wilting point, while Z_r is the soil root depth (Fig. 3). The volume of water in T1 is updated at each time step (S_1^t), considering the volume of water in the previous time step, the amount of rainfall that enters the static storage (D_1) and its maximum capacity in the following way:

$$S_1^t \langle \text{mm} \rangle = \text{Min} (S_1^{t-\Delta t} + D_1, S_{1\max}) \quad (3)$$

The only outflow from this storage is real evapotranspiration (E_t). A similar approach to that used by Edijatno and Michel (1989), Bergström (1995) and Singh and Dickinson (1975) is used in the model, where real evapotranspiration is a function of static storage content, the maximum capacity of T1, potential evapotranspiration (EVP) and an exponent that varies between 0.5 and 1. Vélez (2001) has proposed an exponent of 0.6 for tropical environments. Potential evapotranspiration was estimated using

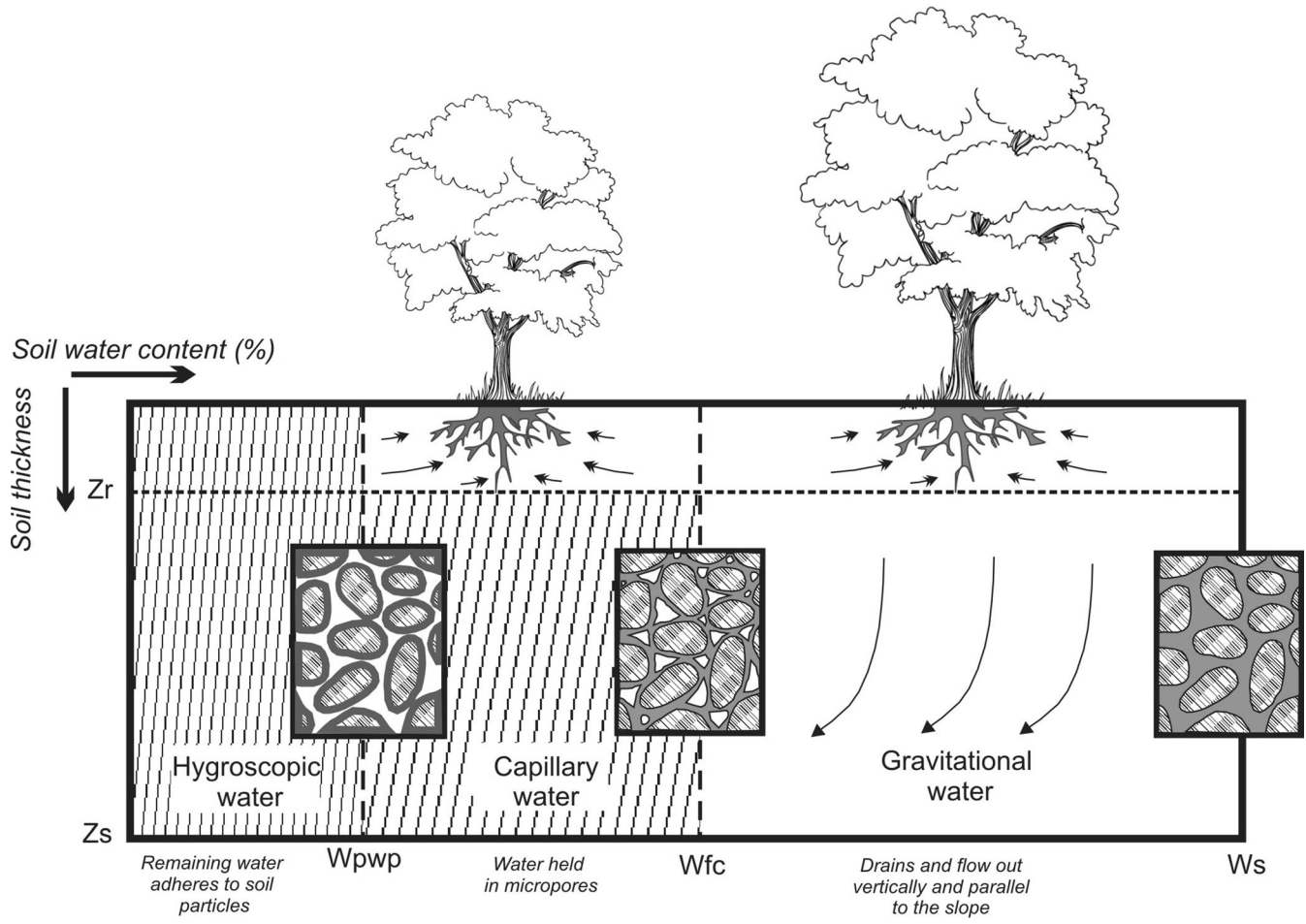


Fig. 2 Water content into the soil and water available. Root depth (Z_r), soil thickness (Z_s), permanent wilting point (W_{pwp}), field capacity (W_{fc}) and saturation (W_s)

the equation proposed by Jaramillo (2006) for the Colombian Andean.

$$E_1 \langle \text{mm} \rangle = \text{Min} \left\{ \text{EVP}^* \left(\frac{S_1^t}{S_{1\max}} \right)^{0.6}, S_1^t \right\} \quad (4)$$

At the end of each time step, the volume of water in T1 updates considering the outflows (E_1):

$$S_1^{t+\Delta t} \langle \text{mm} \rangle = S_1^t - E_1 \quad (5)$$

The second tank (T2) is called *surface storage* and represents water on the hill's sloped surface that is flowing over the slope and has not infiltrated. The amount of water that continues down the slope is the excess of water not in the static storage:

$$R_2 \langle \text{mm} \rangle = R_1 - D_1 \quad (6)$$

The volume of water that enters surface storage (T2) during a time interval is:

$$D_2 = R_2 - R_3 \quad (7)$$

where R_3 is the amount of water that infiltrates into the soil. The volume of water in T2 is updated for each time step in the

following manner:

$$S_2^t = S_2^{t-\Delta t} + D_2 + Z_3 \quad (8)$$

where $S_2^{t-\Delta t}$ is the volume of water in the previous time step in T2, and Z_3 is the excess water from tank 3.

The overland flow at each cell is represented by a non-linear approach using different proposals from several authors. Most authors have recommended a uniform flow such as the Manning equation, where the slope of the energy line is similar to the slope angle of the terrain (Vélez 2001). In this way, the equation for overland runoff velocity is a function of the transversal flow section (A), slope angle (β) and Manning coefficient (n):

$$V_2 = \frac{\xi A^{(2/3)e_1} \beta^{1/2}}{n} \quad (9)$$

where ξ and e_1 are parameters associated with the surface type. For flows over natural terrains, Parsons et al. (1994) have recommended values of 0.038 and 0.315, respectively. The outflows of this tank to the downstream cell according to the overland flow velocity (V_2) are:

$$E_2 = A V_2 \frac{\Delta t}{\Delta x^2} \quad (10)$$

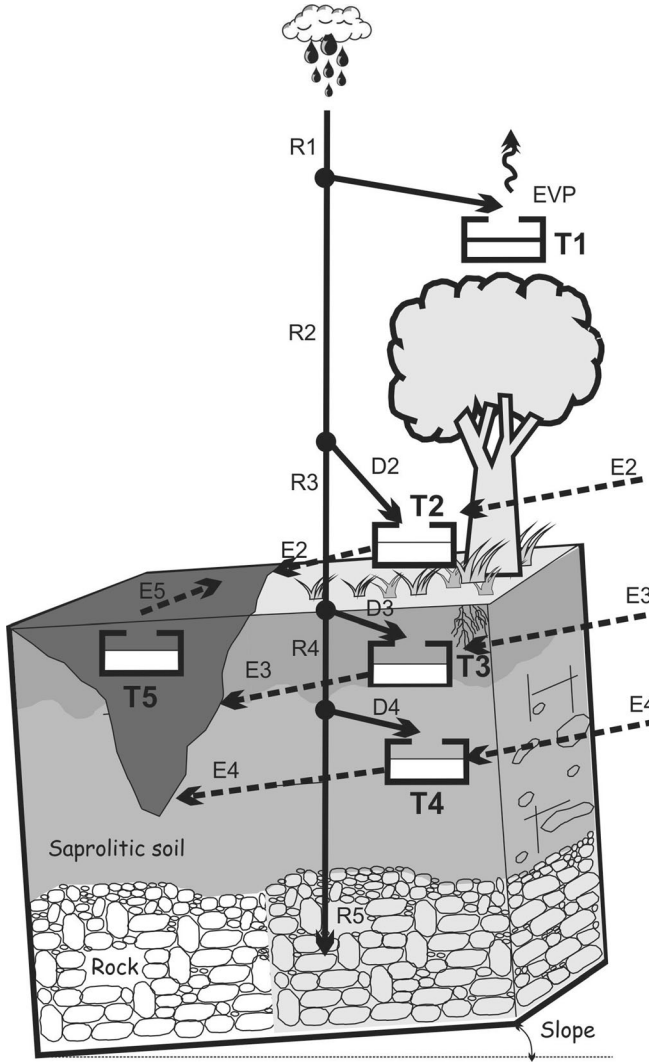


Fig. 3 Hydrological conceptual model. Static storage (T_1), surface storage (T_2), gravitational storage (T_3), aquifer (T_4), channel (T_5), rainfall (R_1), exceedance (R_2), infiltration (R_3), percolation (R_4), groundwater outflow (R_5), overland flow (E_2), subsurface flow (E_3), base flow (E_4), stream flow (E_5), inflow to the tanks ($D_{1:5}$) and evapotranspiration (EVP)

where Δt is the time interval and Δx the grid cell length.

The volume of water ($S_2^{t+\Delta t}$) in T_2 is updated considering the outflows (E_2) are similar to those for tank 1 in Eq. (5).

The third tank (T_3) represents the *gravitational water storage* in the residual soil between field capacity and saturation. This tank models the water column due to subsurface flow parallel to the slope surface through the soil layer and into the drainage system. After ponding the static storage tank (T_1), the infiltration capacity can be approximated by the upper soil saturated hydraulic conductivity (Fig. 5). The amount of water that continues and infiltrates into the soil is then

$$R_3 = \text{Min}(R_2, \Delta t K_s) \quad (11)$$

where K_s is the saturated hydraulic conductivity of the residual soil. In this way, infiltration is controlled by the hydraulic conductivity and the capacity of the residual soil to receive more water. The volume of water that flows into T_3 during a time interval is

$$D_3 = R_3 - R_4 \quad (12)$$

The maximum capacity of T_3 is a function of the volumetric soil moisture content at the saturation point (W_s) and at field capacity (W_{fc}), along with the soil root depth:

$$S_{3\max} = (W_s - W_{fc})Z_r \quad (13)$$

The volume of water in T_3 is then

$$S_3^t = \text{Min}\left(S_3^{t-\Delta t} + D_3; S_{3\max}\right) \quad (14)$$

where $S_3^{t-\Delta t}$ is the volume of water in T_3 at the end of the previous time step. If the capacity of tank 3 is full, then an excess is produced that enters the overland runoff according to:

$$Z_3 = \max\left(0; S_3^t + D_3 - S_{3\max}\right) \quad (15)$$

Subsurface flow velocity is estimated according to Kubota and Sivapalan (1995) as a lateral subsurface flow in mountainous terrains covered by forests:

$$V_3 = \frac{K_s \sin \beta}{(b+1)(S_{3\max})^b} (S'_3)^b \quad (16)$$

where K_s is the saturated hydraulic conductivity of the residual soil, β is the slope angle and b is dependent on the soil type. Kubota and Sivapalan (1995) have used $b=2$ for a mountain basin covered by forest that represents a non-homogeneous hydraulic conductivity along the weathering profile. The outflow of this tank (E_3) and the updated volume of water ($S_3^{t+\Delta t}$) in T3 are calculated similarly to those for tank 2 in Eqs. (5) and (10).

The fourth tank (T4) corresponds to the *aquifer*, where vertical flow represents the system's groundwater outflow and horizontal flow represents the base flow. The model considers the portion of water entering the aquifer that is not incorporated into the basin's base flow, although this amount is very small in most basins and could be excluded from the model. The volume of water that percolates to the saprolite is

$$R_4 = \text{Min}(R_3, \Delta t K_p) \quad (17)$$

where K_p is the saturated hydraulic conductivity of the saprolitic soil. The volume of water that flows into T4 during a time interval is

$$D_4 = R_4 - R_5 \quad (18)$$

The volume of water in T4 is updated for each time step in the following manner:

$$S_4^t = S_4^{t-\Delta t} + D_4 \quad (19)$$

A continuity equation is applied to estimate the outflow from this storage to the downstream cell, assuming a constant velocity. Consequently, the outflow is given by a linear reservoir equation in which the constant velocity can be related to the aquifer's saturated hydraulic conductivity:

$$E_4 = \alpha S_4^t = \left(1 - \frac{dx}{v_4 dt + dx}\right) S_4^t \quad (20)$$

In addition, the volume of water in T4 is updated, accounting for outflows during this time interval:

$$S_4^{t+\Delta t} = S_4^t - E_4 \quad (21)$$

Finally, the volume of groundwater outflow is

$$R_5 = \text{Min}(R_4, K_{pp}) \quad (22)$$

where K_{pp} is the groundwater outflow that can be understood as water losses.

The final tank (T5) represents the *stream flow channel* at the cell level, where each cell is connected to the downstream cell according to the drainage network. T5 also models the flow of water in the drainage basin. Only the ephemeral and perennial channel grid cells contain a T5 tank, while slope grid cells do not.

The propagation of channel flowing to the outlets of an overland, subsurface flow and base flow is collected by the river channel network represented by T5.

The routing along the channel network is carried out at a non-stationary velocity using the geomorphological kinematic wave (GKW) proposed by Vélez (2001). The GKW is a simplification of the Saint Venant equations, in which inertial and pressure terms are neglected. Assuming prismatic canals with constant sections along the reach, the discrete continuity equation can be expressed in terms of the two unknowns, water velocity (V_t) and cross section (A_t), as

$$A_t \Delta x + V_t A_t \Delta t = I_t + S_{t-1} \quad (23)$$

where S represents the volume of water in the channel reach and I_t is the total of the input flows from the connected hillside slopes (overland flow, subsurface and/or base flow) and/or upstream flow from the river channels. The GKW simplification assumes that the energy line slope is equal to the slope of the river bed. The flow velocity and flow cross section can then be directly related by Manning's equation. According to Manning's equation, water velocity is expressed in terms of the flow section's top width (W_t), which is a function of the cross section (A_t), the roughness coefficient (n) and the slope of the river bed (β):

$$v_t = \frac{1}{n} \left(\frac{A_t}{W_t} \right)^{2/3} \beta^{1/2} \quad (24)$$

The channel's hydraulic characteristics (geometry and slope) control the velocity at each reach and time step. The slope of each cell can be easily computed from a digital elevation model (DEM). Unfortunately, it is not economically feasible to measure the channel's geometry for all cells in practice. The GKW uses the Leopold and Maddock (1953) correlation, which relates the cross-sectional geometry and velocity to the river's discharge using potential equations:

$$y = bQ^\delta, \quad w = cQ^\alpha, \quad v = pQ^\lambda \quad (25)$$

where w is the channel width; y is the flow depth; v is the flow velocity; Q is the flow discharge; and the coefficients b , c and p and the exponents δ , α and λ are constant at the regional scale. The hydraulic variables, width, depth and velocity satisfy the continuity equation for rectangular channels:

$$Q = ywv \quad (26)$$

Therefore, the coefficients and exponents in Eq. (25) satisfy the following equations:

$$bcp = 1, \quad \delta + \alpha + \lambda = 1 \quad (27)$$

There are two groups of values for these coefficient and exponents. One group is called the *downstream equations*, which give the relationships for the bankfull discharge (Q_b) along the river network, and the second group, called the *at-site equations*, give the relationships for a given cross section.

Leopold et al. (1964) have proposed a potential relationship between bankfull discharge (Q_b) and the drainage area (A), for a region with climatically and geomorphologically homogeneous

conditions, to a particular cell of the form

$$Q_b = k A^\varphi \quad (28)$$

where k and φ are constant at the regional scale. Incorporating Eq. (28) into the downstream hydraulic geometry equations, it is possible to establish a relationship between the cross section or flow velocity and the drainage area:

$$y_b = b_1(kA^\varphi)^\delta, \quad w_b = c_1(kA^\varphi)^\alpha, \quad v_b = p_1(kA^\varphi)^\lambda \quad (29)$$

Substituting the hydraulic geometry relationships associated with the dominant flow controlling the channel dimensions for the values obtained in Eq. (29) in a function of the drainage area, it is possible to obtain the following expressions:

$$y = b_1 k^{(\delta_1 - \delta_2)} A^{\varphi(\delta_1 - \delta_2)} Q^{\delta_2}, \quad w = c_1 k^{(\alpha_1 - \alpha_2)} A^{\varphi(\alpha_1 - \alpha_2)} Q^{\alpha_2}, \quad v = p_1 k^{(\lambda_1 - \lambda_2)} A^{\varphi(\lambda_1 - \lambda_2)} Q^{\lambda_2} \quad (30)$$

To estimate roughness, several authors have proposed equations that consider sediment size, relative roughness, slope channel, flow depth and cumulative drainage area (Strickler 1923; Limerinos 1969; Hey 1979; Hack 1957; Bray 1979). Considering these approaches, Vélez (2001) and Frances et al. (2007) have proposed a general equation in terms of the slope (β) and the height of the water (y):

$$n = c_n c_d^\varepsilon y^{\varepsilon\theta} \beta^{\varepsilon\theta} \quad (31)$$

where the coefficients c_n and c_d and the exponents ε and θ are constant regional parameters. Substituting Eqs. (30) and (31) in Eq. (24) and solving for velocity, an equation is obtained for the velocity of the water in the channel as a function of the channel geometry and the terrain's geomorphology:

$$V_5 = \left[\frac{A^{\left(\frac{2}{3}-\varepsilon\theta\right)(1-\alpha_2)} \beta^{\left(\frac{1}{2}-\varepsilon\theta\right)}}{c_n c_d^\varepsilon \left(c_1 k_1^{(\alpha_1 - \alpha_2)} A^{\phi(\alpha_1 - \alpha_2)} \right)^{(2/3-\varepsilon\theta)}} \right]^{\frac{1}{1+\alpha_2(2/3-\varepsilon\theta)}} \quad (32)$$

This equation is simplified as

$$V_5 = K_2 A^{w_1} A^{w_2} \beta^{w_3} \quad (33)$$

where

$$K_2 = c_n c_d^\varepsilon \left(c_1^{(2/3-\varepsilon\theta)} k_1^{(2/3-\varepsilon\theta)(\alpha_1 - \alpha_2)} \right)^{-w} \quad (34)$$

$$w = \frac{1}{1 + \alpha_2 \left(\frac{2}{3} - \varepsilon\theta \right)} \quad (35)$$

$$w_1 = w \left(\frac{2}{3} - \varepsilon\theta \right) (1 - \alpha_2) \quad (36)$$

$$w_2 = -w^\varphi \left(\frac{2}{3} - \varepsilon\theta \right) (\alpha_1 - \alpha_2) \quad (37)$$

$$w_3 = w \left(\frac{1}{2} - \varepsilon\theta \right) \quad (38)$$

The GKW requires nine independent exponents and coefficients, which can be obtained from a geomorphological regional study of hydrologically homogeneous zones. However, empirical

studies have been performed by multiple authors that propose different values according to local conditions (e.g. Vélez 2001; Frances et al. 2007, 2012).

Table 1 shows the constant regional parameter range values proposed by Vélez (2001) and Frances et al. (2007). It is important to note that hydraulic geometry relationships correspond to empirical power functions and assume steady, uniform river flow and that the river tends to attain a state of equilibrium or quasi-equilibrium. Therefore, the correlations show a high range of variability depending on whether the assumptions are fulfilled (Singh 2003). To improve the correlations, it is necessary to identify appropriate coefficients and exponents using homogeneous hydrological environments.

Slope stability analysis

Based on the hydrological component, the stability conditions associated with the positive pore water pressure are constrained by the height of the perched water table. To evaluate the slope stability, SHIA_Landslide calculates the perched water table height for each cell and each time step and compares it with the critical landslide-triggering saturated depth value (Z_{wcrit}). For this evaluation, if the residual soil has limited thickness compared to the length of the slope, an infinite slope stability hypothesis can be assumed in the analysis (Fig. 4).

The term 'infinite slope' represents a uniform slope of a suitably large extent, where a typical element can be considered representative of the slope as a whole. Irregularities at the toe and the crest of the slide can be ignored, and soil properties and pore water pressures at any given distance below the ground surface are assumed constant (Graham 1984).

The one-dimensional infinite slope stability analysis is the most common approach to modelling slope failure within a distributed catchment scale framework. This analysis is based on a simplified landslide geometry that assumes a planar slip surface on a planar slope that has been infinitely extended both laterally and distally. The analysis assumes that the slip surface is parallel to the ground surface and coincident with the impermeable substrate and that the perfectly rigid plastic rheological model holds for the soil.

The soil is subject to two major opposing influences: the down-slope component of soil weight, which shears the soil along a potential failure plane parallel to the slope, and the resistance of the soil to shearing. The relationship between these two influences is expressed as a factor of safety.

The shear strength of the soil along the potential failure plane is given by the Mohr-Coulomb failure criterion, and the downslope shear stress (τ) must not exceed the shear strength (τ_f) of the clay.

$$\tau_f = c + \sigma_n \tan\phi \quad (39)$$

The safety factor of the slope can be defined in terms of effective stresses as

$$FS = \frac{c' + (YZ\cos^2\beta - u)\tan\phi}{YZ\sin\beta\cos\beta} \quad (40)$$

When a slope is subject to increased pore pressure due to infiltration or rising of the perched water table, the total stresses and shear stresses remain essentially constant, but the effective stresses, and more specifically the mean effective stress, decrease.

Table 1 Geomorphological kinematic wave parameter ranges proposed for the model

Propagation parameter	Range	Adopted
K_1	0.5–0.75	0.6
φ	0.65–0.8	0.75
c_1	0.5–5.75	3.26
α_1	0.34–0.55	0.5
α_2	0.05–0.2	0.2
c_d	0.5–50.0	20
θ	0.5–2.75	1.26
c_n	0.025–0.07	0.047
ε	0.125–0.18	0.1667

The effective stress principle states that the total stresses applied to soils are supported by the sum of the effective interparticle stresses and neutral pore water pressure (Graham 1984).

According to Graham (1984), natural slopes with steady subsurface flows parallel to the slope and the perched water level at distance Z_w above the slide surface have a pore water pressure of $\mu = \gamma_w Z_w \cos^2 \beta$, and therefore

$$FS = \frac{c' + (\gamma Z - \gamma_w Z_w) \cos^2 \beta \tan \phi}{\gamma Z \sin \beta \cos \beta} \quad (41)$$

The limit equilibrium condition of the slope then occurs when (e.g. Montgomery and Dietrich 1994)

$$c' + (\gamma Z - \gamma_w Z_w) \cos^2 \beta \tan \phi = \gamma Z \sin \beta \cos \beta \quad (42)$$

This equation, solved for Z_w , provides a critical value for the landslide-triggering saturated depth (e.g. D'Odorico and Fagherazzi 2003):

$$Z_{w\text{crit}} = \frac{\gamma}{\gamma_w} Z \left(1 - \frac{\tan \beta}{\tan \phi} \right) + \frac{c'}{\gamma_w \cos^2 \beta \tan \phi} \quad (43)$$

The hydrological component of SHIA_Landslide provides the water content in gravitational storage, and this value must be transformed considering the soil's water content. In this way, according to Fig. 4, the perched water table height is

$$Z_w = \frac{S_3}{(W_s - W_{fc})} \quad (44)$$

However, the minimum (Z_{\min}) and maximum (Z_{\max}) residual soil thickness are computed beforehand to increase the model's computational efficiency. This process identifies the cells where the stability state is independent of the water content: (a) unconditional stable grid cells and (b) unconditional unstable grid cells. These cells are not considered in the slope stability analysis.

On the one hand, because the saturated depth is necessarily smaller than the residual soil thickness ($Z_w \leq Z$), the deposit is always stable when $Z < Z_{\min}$, independently of rainfall (Iida 1999). Equation (42), solved for $Z_w = Z$, provides the immunity depth:

$$Z_{\min} = \frac{c'}{\gamma_w \cos^2 \beta \tan \phi + \gamma \cos^2 \beta (\tan \beta - \tan \phi)} \quad (45)$$

On the other hand, for a certain soil thickness value Z_{\max} , the saturated depth necessary to trigger a landslide is zero and the soil is always unstable, regardless of rainfall occurrence (Iida 1999). The soil is then always unstable at soil thicknesses greater than Z_{\max} . Z_{\max} is determined by setting $Z_w = 0$ in Eq. (42):

$$Z_{\max} = \frac{c'}{\gamma \cos^2 \beta (\tan \beta - \tan \phi)} \quad (46)$$

It is also necessary to find the maximum value of the slope angle (β_o), where the slope is always stable because a saturated depth larger than the soil thickness would be needed to trigger a landslide. β_o is identified when $c' = 0$ and $Z_w = Z$ in Eq. (42). When $\beta < \beta_o$, the slope is always stable.

$$\beta_o = \tan^{-1} \left[\tan \phi \left(1 - \frac{\gamma_w}{\gamma} \right) \right] \quad (47)$$

Figure 5 shows the flow diagram structure of the coupled model, SHIA_Landslide, delineating the steps used in the hydrological and slope stability calculations.

Measures of validity

SHIA_Landslide provides the root mean square error (RMSE) and Nash-Sutcliffe efficiency coefficient (NS) when the user enters the observed stream flow data in the model.

The RMSE measures the average magnitude of the error on a scale ranging from 0 to infinity, with 0 being a perfect score. The RMSE of a prediction model with respect to the estimated variable (Q_{obs}) is defined as the square root of the mean squared error:

$$\text{RMSE} = \sqrt{\frac{\sum_{t=1}^T (Q_{\text{obs}} - Q_{\text{sim}})^2}{T}} \quad (48)$$

where Q_{obs} is the observed, Q_{sim} is the modelled discharge at time t and T is the time horizon.

The NS is commonly used to assess the predictive power of hydrological discharge models. Nash-Sutcliffe efficiencies can range from $-\infty$ to 1. An efficiency of 1 corresponds to a perfect

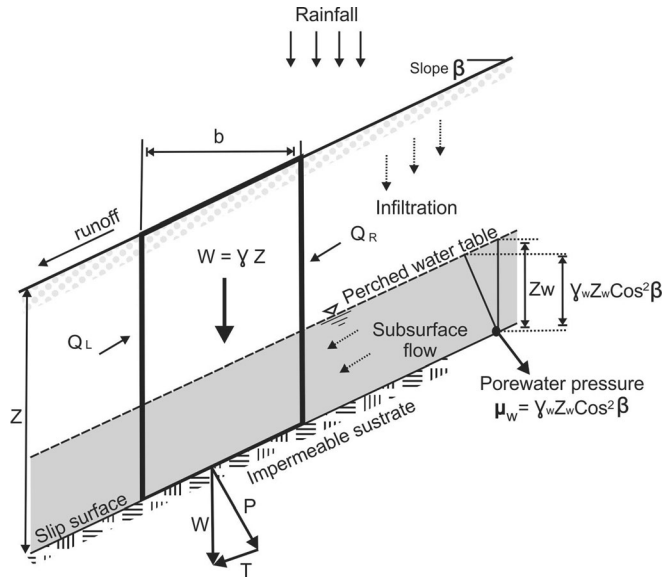


Fig. 4 Geotechnical conceptual model proposed. γ is the soil bulk density, γ_w is the water density, Z_w is the saturated soil thickness above the slip surface, Z is the soil thickness measured vertically, β is the gradient of the hillslope, and Q_L and Q_R are the resultant forces on the sides of the slice

match between the model and observations, while an efficiency of 0 indicates that the model predictions are as accurate as the mean of the observed data and an efficiency less than 0 ($-\infty < NS < 0$) occurs when the observed mean is a better predictor than the model.

$$NS = 1 - \frac{\sum_{t=1}^T (Q_{obs} - Q_{sim})^2}{\sum_{t=1}^T (Q_{obs} - \bar{Q}_{obs})^2} \quad (49)$$

where \bar{Q}_{obs} is the mean of the observed discharge. SHIA_Landslide also calculates the balance of water in percentage terms for both RMSE and NS. The model uses the total rainfall over the catchment and the outflows along the different grid cells for balance and considers the water storage in the tanks at the end of the simulation. The water balance is obtained as follows:

$$WB(\%) = \frac{\text{Outflows} + \text{EVP} + \text{Storage} - \text{Rainfall}}{\text{Outflows} + \text{EVP}} \quad (50)$$

Model parameters

Regarding the morphometric and soil parameters required for SHIA_Landslide, the program operates on a gridded elevation model of a map area and accepts the input parameter maps from a series of ASCII text files. Landslide-controlling parameter maps are allowed to vary over the grid area, making possible the analysis of complex rainfall events over complex terrains. SHIA_Landslide considers three morphometric input parameter maps, namely accumulated area, flow direction and slope angle; and nine soil input parameter maps, namely soil thickness, cohesion, saturated unit soil weight, friction angle, saturated hydraulic conductivity of residual soil, saturated hydraulic conductivity of saprolitic soil, saturated hydraulic conductivity of rock, maximum static water

storage and maximum gravitational water storage (Table 2). Soil input parameter maps are adjusted using correction factors.

Correction factors

For the calibration procedure, the split parameter procedure for distributed modelling proposed by Frances et al. (2007) has been implemented. The effective parameters for the model at each cell are split into two components, a hydrological or geotechnical characteristic and a correction factor common to all cells that accounts for all modelling errors. Correction factors account for time and space scale effects together with the model and input errors, leaving the hydrological or geotechnical characteristics free of these problems while maintaining the parameter's physical meaning (Frances et al. 2012).

Initially, the maps are estimated a priori using environmental and available information. Then, correction factors are used to modify globally the previously estimated maps. In this way, the spatial variability captured in the initial estimated maps is kept and a global change in magnitude of parameter maps is performed with correction factors (Frances et al. 2007). Such factors are applied globally to soil input parameter maps instead of to each cell value in the calibration maps, drastically reducing the number of factors to be calibrated. This strategy allows for fast and agile modification of different hydrological and geotechnical processes.

Frances et al. (2007, 2012) have established a general search range for the correction factors. Values around unity can be expected for the correction factors of the maximum static and gravitational storage capacity, depending on the errors in the initial estimation of the catchment characteristics, the model inputs and the model itself. Cohesion, friction angle and soil thickness are also included in this range, with values around unity. Due to the high degree of non-linearity in those processes with a threshold capacity, the scale effects will produce infiltration and percolation values of less than unity, but macropore structures could increase these values (Table 2).

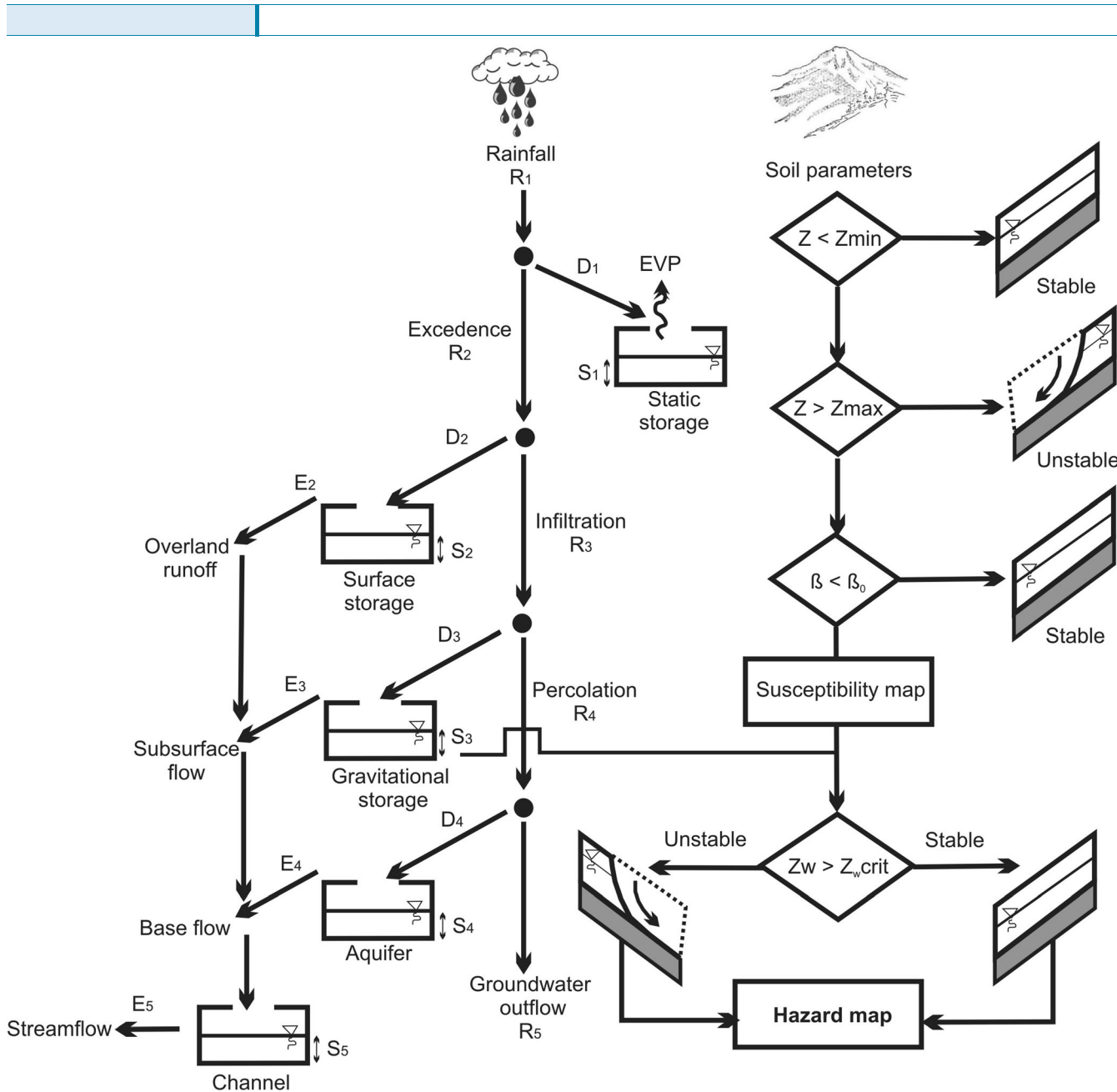


Fig. 5 SHIA_Landslide model

Additional to the soil input parameter maps, the surface, subsurface, base and channel flow velocities are also adjusted by correction factors. Concerning the correction factor for the base flow, the basic characteristic used in the model is the vertical saturated hydraulic conductivity of the upper soil substratum, and because the horizontal saturated hydraulic conductivity is usually one or two orders of magnitude higher than the vertical conductivity, a wide range should be expected for the base flow velocity, between 1 and 1000. The subsurface velocity has similar results, but the existence of the macropore structures means that the correction value can be expected to have a value between 10 and 1000. In terms of the groundwater outflow, uncertainty should be expected without proper knowledge of the groundwater balance and the correction value could have any value between 0 and 10.

The search range for the correction factors of the surface runoff velocity and channel velocity is limited to values between 0 and 2 depending on the spatial variability and data uncertainty (Table 3).

The split parameter structure to calibrate a model requires a substantial hydrological knowledge of the catchment in order to limit the correction factors to the proper solution and to determine an initial wide search range for the correction factors.

Case study

Site description

La Arenosa is located 160 km east of the Aburrá Valley, on the south-eastern side of the Central Cordillera in the Antioquia region. The catchment is part of the upper San Carlos River Basin

Table 2 Model split parameter structure and correction range values proposed by Vélez (2001) and Frances et al. (2007) for soil input parameter maps

Cell parameter	Correction	Decomposition	Range	Adopted
Maximum static water storage ($S_{1\max}$)	C_1	$S_{1\max}^*=C_1 S_{1\max}$	[~1.0]	0.1
Maximum gravitational water storage ($S_{3\max}$)	C_2	$S_{3\max}^*=C_2 S_{3\max}$	[~1.0]	1.0
Sat. hyd. conductivity of residual soil (K_s)	C_3	$K_s^*=C_3 K_s$	[~1.0]	4
Sat. hyd. conductivity of saprolitic soil (K_p)	C_4	$K_p^*=C_4 K_p$	[~1.0]	0.5
Sat. hyd. conductivity of rock (K_{pp})	C_5	$K_{pp}^*=C_5 K_{pp}$	[0.0–10.0]	0
Cohesion (c')	C_6	$c'^*=C_6 c'$	[~1.0]	1.45
Friction angle (ϕ)	C_7	$\phi^*=C_7 \phi$	[~1.0]	1.15
Saturated unit soil weight (γ)	C_8	$\phi^*=C_8 \phi$	[~1.0]	1.0
Soil thickness (Z_s)	C_9	$Z_s^*=C_9 Z_s$	[~1.0]	0.8

and is formed by the confluence of the La Arenosa and Betulia rivers, with an area of 9.91 km². The area's elevation ranges between 1000 and 1900 m a.s.l. The basin is highly dissected, with hillside slope lengths on the order of 40–60 m. Most of the land area has slope angles ranging from 20° to 40° (Fig. 6).

The area has a tropical humid climate with a mean annual precipitation of 4300 mm and a mean annual temperature of 23 °C (IGAC 2007). The precipitation regime is dominated by high variability at both the interannual and interseasonal scales. Monthly rainfall distributions reveal a seasonal pattern, with a clear difference between the rainy seasons that extend from September to November and from March to May and the dry season, which yields a minimum rainfall level in July.

The geology of the study area consists of residual soils from granodiorite rocks covered in the gently sloping areas with slopes and fluviotorrential deposits. The dominant granitic component is grey and medium to coarse-grained, consisting of cream or pale yellow feldspar, smoky quartz and smaller proportions of reddish-brown biotite and dark hornblende. These rocks have been severely weathered in situ. The progressive spheroidal decomposition of the granite has been rapid and extensive, with an average weathering depth of 30 m due primarily to chemical decomposition under the humid tropical climate (Mejía and Velásquez 1991).

The saprolite is fairly well graded as sandy silt to silty sand in texture, with some gravel and small amounts of clay. Relict joints of the parent rock are preserved in the saprolite zone and can significantly alter the observed hydraulic conductivities of the surrounding soil matrix (INTEGRAL 1990).

The September 21st, 1990 rainstorm in the La Arenosa catchment

A short-duration, high-intensity rainfall event affected the basin of La Arenosa on 21 September 1990. In less than 3 h, a precipitation of 208 mm fell within the study area, triggering many landslides. The September 21, 1990 event is unique considering the huge number of failures that took place as a result (Fig. 7).

The area's population was strongly affected during this event: 20 people were killed and 260 had to be evacuated, 27 houses were destroyed and 30 others were damaged and several bridges and more than 100 m of highway were ruined. The Calderas Hydro-power Energy Plant was flooded and severely damaged by large blocks carried along the La Arenosa stream. The total losses were estimated at more than US \$6 million (Hermelin et al. 1992).

Prolonged low-intensity precipitation had characterised the two preceding months, resulting in approximately 621 mm of rain. The statistical analysis of historical rainfall carried out by Mejía and Velásquez (1991) indicated that the event was exceptional, according to the rain gauge of San Carlos, with a return period of 200 years.

Analysis of post-event aerial photos and field investigations allowed for a partial reconstruction of the pattern and characteristics of the landslides in the La Arenosa catchment. INTEGRAL (1990) and Mejía and Velásquez (1991) have offered a detailed landslide inventory and a comprehensive description of the landslides triggered during the event (Fig. 6).

Mejía and Velásquez (1991) report 838 soil slips in the entire upper basin for the San Carlos River. Most of these slips transformed into debris flows; 699 landslides were reported in the La Arenosa catchment, and all were classified as soil slips and mud/debris flows ranging from very to extremely rapid, with high water content.

The landslides commenced as shallow translational slides. After the initial mobilisation, a rapid displacement occurred in a chaotic mixture, containing a variable amount of water that scoured the residual soil and vegetation downwards while incorporating soil and bedrock fragments. The movement evolved along the slopes under a quasi-viscous flow at high speed, increasing the sediment transport for superficial erosion along the channels.

The landslide bodies were small with respect to the flow length and slip surface parallel to the slope surface. Field studies showed that the depth of the failure surface was approximately 0.6–1.5 m and corresponded to the contact residual soil or saprolite. In all observed cases, the failure surface matched the contact area of the residual soil with the underlying saprolite (Mejía and Velásquez 1991).

Digital terrain model

A digital elevation dataset with submetre resolution was obtained from aerial photographs provided by the Instituto Geográfico Agustín Codazzi (IGAC). Spatial discretisation of the model was obtained, splitting the study area into a number of squared grid elements with a raster size of 10 m according to the DTM (Fig. 6). Morphometric parameters such as slope angle, flow direction and flow accumulation were calculated using the DEM and ArcGIS 10.1 hydrological tools.

Table 3 Model split parameter structure and correction range values proposed by Vélez (2001) and Frances et al. (2007) for flow velocities

Surface runoff velocity (V_2)	C_{10}	$V_2^* = C_{10}V_2$	[0–2]	0.025
Subsurface velocity (V_3)	C_{11}	$V_3^* = C_{11}V_3$	[10–1000]	450
Base flow velocity (V_4)	C_{12}	$V_4^* = C_{12}V_4$	[1.0–1000]	50
Channel velocity (V_5)	C_{13}	$V_5^* = C_{13}V_5$	[0–2]	1

Soil properties

Soil properties are strongly related to the parental material, allowing for the assumption that the hydrological and geotechnical soil parameters are uniform within the parental geological units. The catchment presents a rather homogeneous geology characterised by sandy soils with high permeability. The geology of the catchment is defined by two main soil types identified by the Instituto Geográfico Agustín Codazzi (IGAC 2007), Yarumal (YAE1 and YAF2) and the Polanco (POC1) soil association.

For each geological unit, a detailed stratigraphic profile has been constructed to support the definition of geotechnical and hydrological input parameters according to the official soil map (IGAC 2007a). Soil descriptions, field tests and laboratory analyses on soil samples from the La Arenosa catchment were performed by Mejía and Velásquez (1991) and INTEGRAL (1990) after the landslide event. The soil parameters were extended to the entire catchment using this stratigraphic information, the soil typology correlation and field work corroboration. Table 4 shows the soil parameters obtained for the model implementation.

Initial conditions

The initial conditions for the model correspond to the initial water content for each tank. All the tanks were assumed to have 50 % of water content. This percentage represents a value to start the

simulation, and it could be changed considering that when the model starts to run, the tanks gradually incorporate water, and after several time steps, the tanks adjust the water volume according to the rainfall conditions. For that reason, it is necessary to run the model a considerable time before the rainstorm of interest.

To obtain the initial conditions previous to the September 21, 1990 rainstorm, a warm-up period of 3 months previous to this date was used. Although the September 21, 1990 rainstorm occurred over a period of just 3 h, the warm-up period of 3 months was selected considering seasonal patterns to eliminate the influence of initial condition errors.

Calibration and validation procedure

Calibration and validation procedures of the hydrological module were performed using hourly time step rainfall and discharge flow databases available for the catchment during the period of 2007 to 2012. Regarding to the calibration of the geotechnical module, although a detailed landslide inventory was not available for the basin, there were no reported landslides in newspapers or recent landslide scars identified during fieldwork inspections for the period between 2007 and 2012, and the cells identified in the model as unstable were classified as errors or false positives. The September 21, 1990 event was used to validate the geotechnical module and assess the accuracy of the performance of the SHIA_Landslide model.

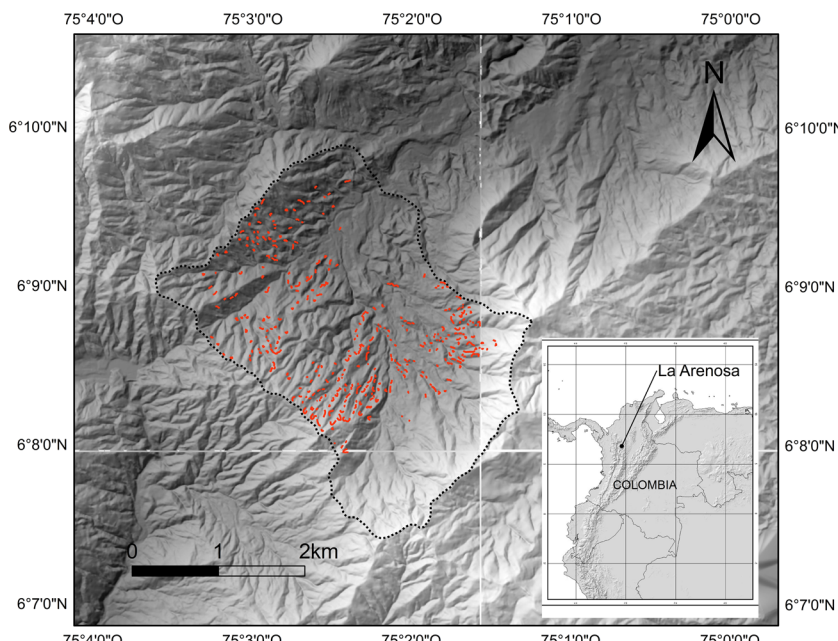


Fig. 6 Location of the La Arenosa catchment, in the southeastern side of the humid tropical and complex terrains of Central Andean Cordillera in Colombia. Red lines show the landslide scars produced by the September 21, 1990 rainstorm according to the Landslide database elaborated by Mejía and Velásquez (1991) and INTEGRAL (1990)

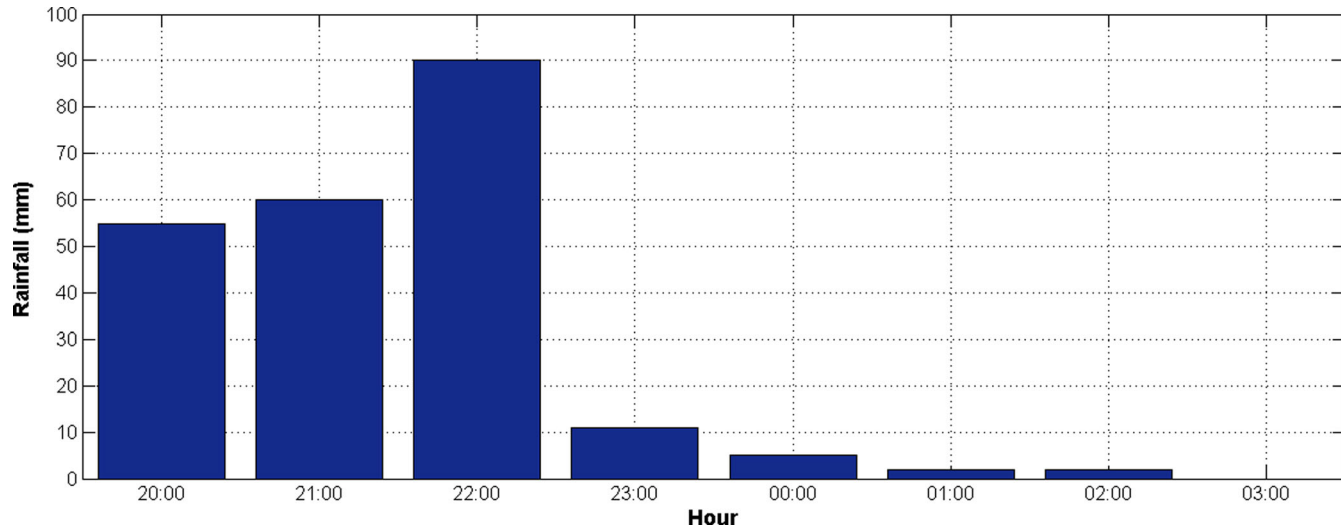


Fig. 7 Hourly rainfall histogram of the September 21, 1990 rainstorm. In less than 3 h, a precipitation of 208 mm fell within the study area, triggering 808 landslides in La Arenosa catchment

Hydrological module

The calibration procedure was carried out in a traditional performance to identify how well the model could reproduce observed data (Klemes 1986). The adjustment of the correction factors for soil input parameters and flow velocities values was conducted by a trial and error process until the output of the model closely matched the observed data. A manual adjustment process was selected because it allowed the evaluation of the contributions and relevance of parameters, making it possible to check and understand the model's structure. The performed calibration process determined the 'best fit' using the RMSE, NS and water balance for the correction factors of hydrological parameters.

The calibration procedure for the hydrological module was conducted for the period March–May/2011, while the September–November/2012 and September–November/2007 periods were used to validate the hydrological module. These specific periods were selected because several rainfall storms occurred within them and permitted a performance evaluation of the model for normal and extreme conditions.

The results of the hydrological module calibration are shown in Fig. 8. The simulated hourly flows resulting from the SHIA_Landslide agreed very well with La Arenosa stream flow. The model predicted flow peaks and slightly under-predicted low flows. A comparison of the predicted and discharge data for La Arenosa suggests that the model provided a good prediction of the landslide hydrology. Most of the peaks were simulated with appropriate time precision, although the model slightly overestimated the stream flow for the highest peaks. In some cases, stream flow overestimation could be originated by infiltration reduction and, consequently, increasing the slope stability. The RMSE (0.292) and the NS (0.852) showed good correlation between the simulated and La Arenosa stream flows, while the water balance showed a low negative difference (WB=−0.9 %).

Model validation is used to indicate the existence of a procedure for analysing simulation performance and verifying the ability of a procedure to accomplish a given scope (Klemes 1986; Biondi et al. 2012). Considering that validation provides a model's goodness of fit that can be expected when the model is applied to

conditions outside of the calibration series, two validation tests were applied for the September–November/2007 and September–November/2012 periods with this model.

The simulated hourly flows agreed well with La Arenosa stream flows for SHIA_Landslide. Despite occasional discrepancies in peak flows, most peaks were predicted correctly. For the period of September 2007 to November 2007, the RMSE was 0.451, the NS was 0.506 and the WB was −0.4 %. The September 2012 to November 2012 period showed slightly higher values, with an RMSE of 0.297, NS efficiency of 0.724 and WB of −0.6 %.

Geotechnical module

The calibration procedure for the geotechnical module was conducted for the period March–May/2011, September–November/2012 and September–November/2007. Similar to the hydrological module, hourly data were also used for geotechnical analysis. Although there is no landslide occurrence database for the catchment, and knowing that the simulated unstable grid cells were considered false positives, the correction factors for geotechnical input parameter maps were adjusted into a range of possible values, reducing the percentage of false positives to less than 1 % of the entire catchment.

In terms of the geotechnical module calibration, the false positives were 0.5 % of the entire catchment for the period of March–May/2011, 0.7 % for the period of September–November/2007 and 1.1 % for the period of September–November/2012.

Receiver operating characteristic analysis and comparison

To assess the accuracy of the model's performance, several previous studies have focused on the rate of successfully predicted landslides but ignore the component of stable areas erroneously classified as unstable. To reach a balanced analysis, a quantitative performance evaluation of SHIA_Landslide was created for the September 21st, 1990 rainstorm event in the La Arenosa catchment through GIS-based map overlay operations and by calculating receiver operating characteristic (ROC) values.

ROC analyses have been used extensively in recent years for comparative evaluations of landslide models (Fawcett 2006). ROC

Table 4 Morphometric and soil input parameters of La Arenosa catchment

Soil parameter	Alluvial soil (POc1)	Residual soil (YAE1–YAF2)
Accumulated area (km^2)	0–9.8	0–5
Flow direction	–	–
Slope angle ($^\circ$)	0–5	0–62
Maximum static storage (mm)	63–135	63–135
Maximum gravitational water storage (mm)	191–465	191–465
Saturated hydraulic conductivity of residual soil (cm/h)	0.479	1.96
Sat. hyd. conductivity of saprolitic soil (cm/h)	0.0799	0.0799
Sat. hyd. conductivity of rock (cm/h)	8×10^{-8}	8×10^{-8}
Cohesion (kPa)	1	5
Friction angle ($^\circ$)	34	24
Saturated unit soil weight (kN/m^3)	20	18
Soil thickness (m)	2.5–2.8	1.2–2.8

analysis for the assessment of landslide model performance is based on the fact that each grid cell can be mapped using actual classes. These classes are called positive and negative class labels, according to landslide inventory databases, and predicted classes, called true and false class labels, produced by a model. A major advantage of ROC analysis is that several metrics have been defined for evaluating the performance of models. During the performance evaluation, sensitivity, specificity, false alarms and precision of the simulations were calculated and used for a quantitative comparison.

The true positive rate, also called hit rate, sensitivity or positive accuracy, is defined as the ratio between true positives and the total actual positives, while the true negative rate, also called specificity or negative accuracy, is the ratio between true negatives and the total actual negatives. The false positive rate, also called the false alarm rate or negative error, is defined as the ratio between false positives and the total actual negatives, and the positive predictive value, also called precision, is the ratio between true positives and the total predicted positives.

Table 5 shows the quantitative performance evaluation of SHIA_Landslide for the September 21st, 1990 rainstorm. According to the analysis, SHIA_Landslide shows a high hit ratio (77 %) and specificity (76 %), suggesting a significant prediction of the failure areas and a relative low false alarm rate (24 %) and precision (0.067), indicating a number of stable areas erroneously classified as unstable.

To compare results effectively, the model developed by Montgomery and Dietrich (1994), called SHALSTAB, was applied to the rainstorm event at La Arenosa using similar values for the parameters involved in SHIA_Landslide (Martínez 2012). SHALSTAB has been widely applied in engineering practice for shallow landslide susceptibility assessment. SHALSTAB, similar to SHIA_Landslide, simulates the fluctuation of a perched water table lying above a slope-parallel impermeable layer controlled by rainfall. Table 6 shows the performance evaluation for both models with the La Arenosa rainstorm. SHIA_Landslide shows a considerably higher hit ratio without a considerable increase in false alarm rate,

specificity and accuracy. The precision and likelihood ratio performances are better for SHIA_Landslide with the La Arenosa rainstorm of September 21, 1990.

Results and discussion

Spatial performance of the model

The model's validation was carried out by analysing predicted landslides with respect to the distribution of triggered landslides on the September 21, 1990 event in the La Arenosa catchment. To evaluate the model's performance, only the scars on landslide inventory maps elaborated by Mejía and Velásquez (1991) and INTEGRAL (1990) were rasterised. Although the inventory maps consisted of landslide polygons, including the depletion and accumulation zone, most of the area actually corresponded to displaced material over areas that did not fail.

The model performance is related to the capacity to predict a relatively small number of unstable pixels. The 350 landslide scars in the landslide inventory correspond to just 2.2 % of the study area. An ideal model performance simultaneously maximises the agreement between known and predicted landslide locations and minimises the area outside the known landslides predicted to be unstable.

Spatial performance was evaluated independently for the susceptibility and hazard maps. Landslide zoning is based on definitions and terminology used in Fell et al. (2008). Landslide susceptibility refers to a quantitative assessment and spatial distribution of landslides that exist or potentially may occur in an area, while landslide hazard takes the outcomes of the landslide susceptibility map and evaluates the temporal occurrence of potential landslides triggered by the simulated rainstorm.

The first product of the model corresponds to the susceptibility map of landslides triggered by rainfall under saturated conditions, for which unconditionally unstable and unconditionally stable areas have been identified before the rainfall event. The stability condition of these areas is a function of cohesion, friction angle, weight unit of the soil and failure surface depth and is independent

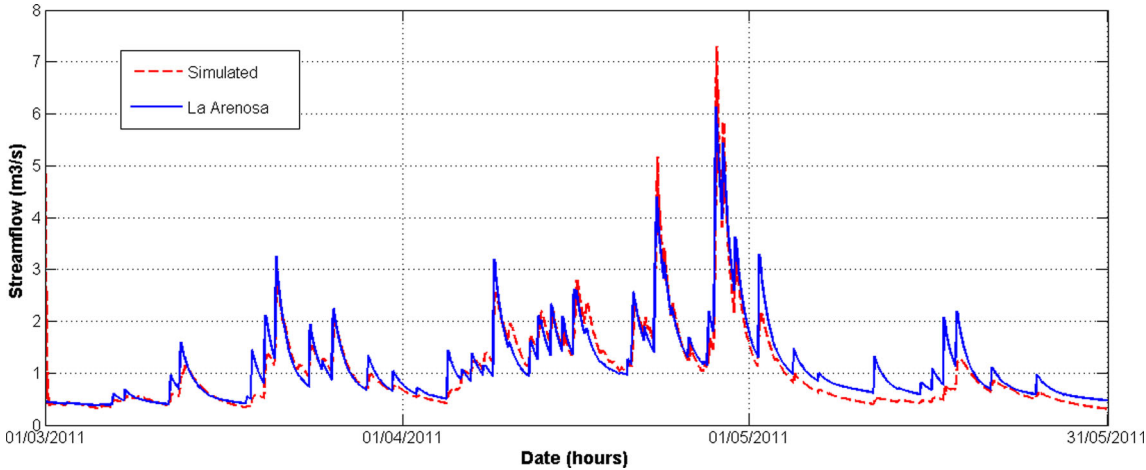


Fig. 8 Results using SHIA_Landslide of simulated hourly discharges at the calibration flow gauge station La Arenosa during the calibration period compared with the discharges obtained for La Arenosa stream

of rainfall. This elimination of grid cells for unconditionally unstable and unconditionally stable areas is not considered during the analysis of the rainfall event. Figure 9 shows the susceptibility map for the La Arenosa catchment. The yellow areas are the potentially unstable areas during landslides triggered by rainfall and correspond to 52 % of the total area.

Unconditionally unstable areas correspond to 1.64 % of the La Arenosa catchment. Most of these areas are located in the lower part of the catchment on the channel bank formed by alluvial sediments. These unstable areas originate from the fluvial erosion of streams over their banks and are not a direct consequence of rainfall occurrence. Another important source is ‘orphan cells’, unstable cells surrounded by stable cells. These areas correspond to specific cells where the DTM shows steep slopes due to the presence of natural or man-made slopes.

Unconditionally stable areas make up 46 % of the total catchment. These areas are located in the lower part of the basin and formed by alluvial sediments with gentle slopes. Such areas are also found along the valley bottoms and crests and are characterised by flat surfaces. The areas are stable during rainfall events due to very low slope angles, where the shear stress does not exceed the shear strength of the soil material.

Potentially unstable areas correspond to 52 % of the total catchment area and correspond to areas that could be affected by landslides during rainstorms. These areas will be checked during the rainfall event modelling.

The computational cost is a function of the time required by the model to run and the hardware used. The susceptibility map obtained by SHIA_Landslide allows computer running time to be conserved, which is essential in an early warning system, and allows the model’s next step to focus only on potentially unstable areas. The total time required for the model to run a period of 2200 h (approximately 3 months) in a catchment composed of 100,000 grid cells is approximately 4–5 min. This time could be a reasonable period for an early warning system but should be evaluated for each specific case.

The potentially unstable areas were located in the upper and middle part of the slopes, which were moderately to extremely steep. Comparing the susceptibility map with the landslide scar

inventory, 92 % of the scar pixels were located in these potential unstable areas. Only 8 % of the scar cells were erroneously identified by the model as unconditionally stable. These areas were checked in the DTM, and most corresponded to boundaries around potentially unstable areas, where, during the digitisation process, landslide scars were extended and included one or, at most, two unconditionally stable neighbouring pixels. Three potential reasons could explain this issue: (i) a digitisation problem during the landslide inventory mapping; (ii) landslide areas that originated through the erosion processes of displaced material from neighbouring unstable areas or by the propagation of a failure surface, not considered in the model; or (iii) particular conditions that were not represented by the DTM (most likely human intervention) and not considered in the model.

Figure 10 shows a hazard map of the areas with landslide occurrences triggered by rainfall. These occurrences are the result of the slopes’ stability conditions under the perched water table and the pore water pressure changes generated by rainfall. The model replicates the activity process observed during field surveys carried out by Mejía and Velásquez (1991) with very good accuracy: 55.3 % of the total watershed of the La Arenosa catchment was potentially unstable under rainfall conditions. In this area, 77 % of the scar pixels were correctly predicted by the model as unstable areas and 1.2 % of the scar pixels were classified as unconditionally unstable areas; 22 % of the scar pixels were erroneously classified by the model as stable. This value included the 8 % of the pixels erroneously classified as stable from the susceptibility map, so in any case it was not possible to identify these cells as unstable during the rainstorm.

Temporal performance of the model

A correct estimation of failure timing is constrained by the capability of the hydrological components to simulate pore pressure responses to hydrological forcing (Carrara et al. 2008). To evaluate the model’s temporal performance, landslide occurrence was checked hourly during the rainstorm to compare it with the reported timing of landslide events. Rain started at 20:00, and 208 mm fell in the next 3 h. Landslides were reported during the night of September 21, and according to Mejía and Velásquez

Table 5 Statistical indexes measuring the performance of SHIA_Landslide

Index	Value	Range
Hit rate	76.98	[0, 100]
False alarm rate	24.24	[0, 100]
Specificity	75.75	[0, 100]
Precision	0.067	—

(1991), most landslides occurred during the second hour of the rainstorm, but there is no detailed temporal record.

At 20:00 local time, 29.4 % of the cells failed, reaching a total percentage of 31.9 % of unstable grid cells. At 21:00, 40.3 % of the cells failed, with a total percentage of 72.3 %, and finally at 22:00, the last 27.7 % of the unstable grid cells failed, reaching 100 %. Using an hourly temporal scale, the model results coherently reproduced the timing of the occurrence, during which most landslides were reported during the first and second hours of the rainstorm.

A fundamental factor affecting the temporal performance of models is the antecedent rainfall. It has been recognised in the literature that antecedent rainfall can be a predisposing factor in the activation of soil slips (Rahardjo et al. 2001). Antecedent rainfall's role in landslides triggered by rainfall has been an interesting debate, and its influence is difficult to quantify because it depends on several factors, including the heterogeneity of soils and the regional climate.

The effect of antecedent rainfall was studied using SHIA_Landslide. The antecedent rainfall during the 90 days prior to the September 21, 1990 rainstorm was increased up to 100 %, and there was no significant change of the slope stability response to the rainstorm observed. Moreover, the increase in antecedent rainfall in the 24 h before the September 21, 1990 rainstorm did not represent any change in the perched water table response during the rainstorm. These results were coherent with the findings of various authors on residual soils with high hydraulic conductivities, characteristic of sandy residual soil from granite rocks.

These results imply that high-permeability soils require only short periods of rainfall before failure occurs and that antecedent moisture conditions do not always play a significant role, in accordance with the observations carried out by Rahardjo et al. (2008), Brand (1985) and Corominas and Moya (1999).

Finally, as part of the simulation analysis, it is possible to establish rainfall thresholds to predict the occurrence of abundant landslides. Rainfall thresholds for this case are defined as the minimum amount of rainfall necessary to trigger an important number of landslides (>1 % of potentially unstable grid cells).

Figure 11 shows the percentage of unstable grid cell that fail due to rainfall, with the maximum percentage obtained tending to be approximately 51 %. There is no significant increase in landslides

for high rainfall peaks (>100 mm/h). This result illustrates an asymptotic relationship between rainfall peaks and landslide occurrence and a tendency to increase linearly for small rainfall peaks, decreasing until it reaches an asymptotic value of approximately 50 %.

Conclusions

SHIA_Landslide is a modelling program for computing positive pore pressure changes and associated changes in factor of safety due to rainfall infiltrations using a conceptual and distributed hydrological module coupled with a physically based and infinite stability slope geotechnical module. It is not considered as fully physically based because the dynamic equations for the flows between different tanks are simplified. However, the model has a physical basis in the sense that its parameters and state variables have a physical meaning and can be measured in the field.

Consequently, SHIA_Landslide represents an innovative approach that introduces new concepts for the simulation of shallow landslides triggered by rainfall. It uses a robust and simple conceptual hydrological model to simulate all the main components of the land phase of the hydrological cycle and to establish the different components of hydrographs at multiple sites. These advantages of the model allow a better understanding of the hydrology of slopes and, consequently, the stability of slopes. SHIA_Landslide can further be distinguished by:

- (a) The capacity to capture surface topography and its effects concerning overland flow and the concentration cells of subsurface flow
- (b) Its use of a DTM to establish relationships among cells, geomorphological parameters, slope angle, direction and other factors
- (c) The incorporation of rainfall datasets with the user's preferred spatial and temporal resolution
- (d) Continuous simulations for long periods of rainfall data (years) or event simulations for specific storms
- (e) Consideration of the effect of horizontal and vertical flow
- (f) Operation at a basin scale
- (g) Inclusion of a complete hydrological water process that permits perched water table calibration
- (h) Consideration of vertical infiltration and horizontal flow in saturated conditions

Table 6 Comparison of SHALSTAB and SHIA_Landslide for La Arenosa rainstorm event (Martínez 2012)

Model	Hit rate	False alarm rate	Specificity	Precision
SHIA_LANDSLIDE	77	24	76	0.06
SHALSTAB	29	21	79	0.05

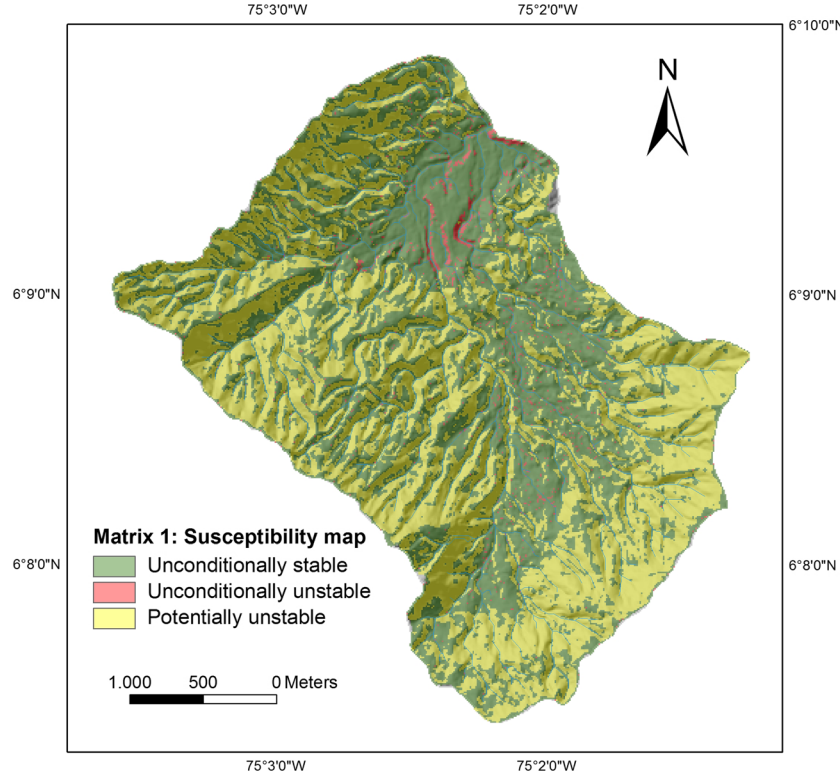


Fig. 9 Susceptibility map obtain for SHIA_Landslide

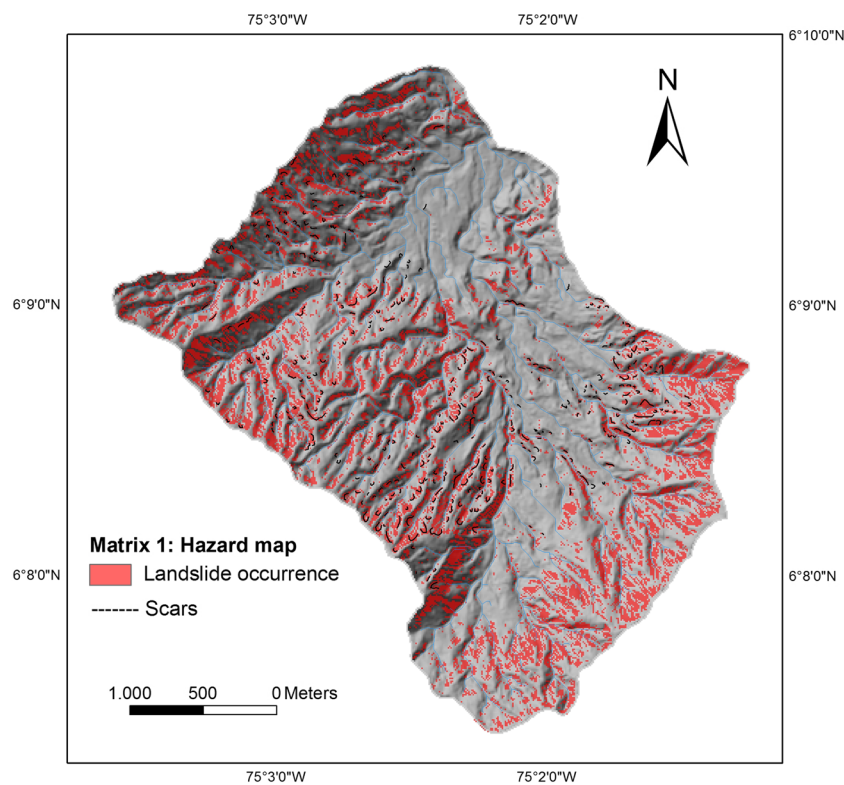


Fig. 10 Areas with landslide occurrence triggered by the September 1990 rainstorm simulated by SHIA_Landslide

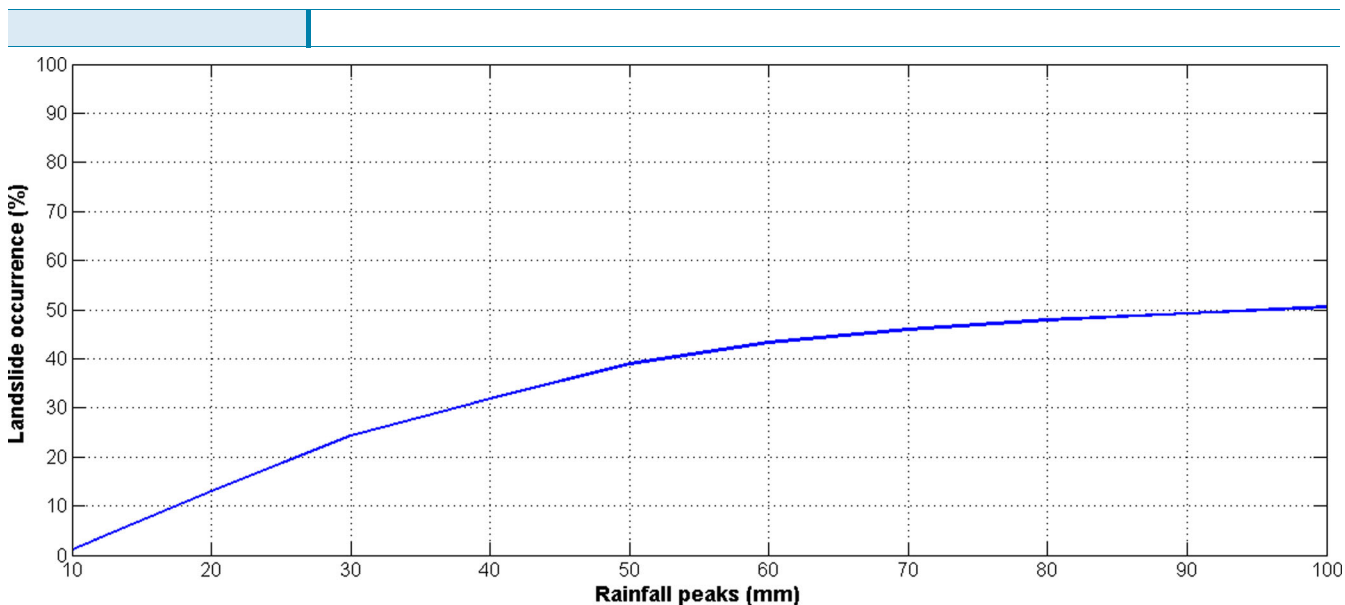


Fig. 11 Percentage of potentially unstable grid cells according to the maximum rainfall peak for La Arenosa catchment

SHIA_Landslide is an interesting tool that can be implemented in the development of early warning systems, aid in providing real-time rainfall monitoring and assist in the dissemination of alerts and communications. This program can also be applied to land-use management and emergency planning as a tool for evaluating landslide susceptibility or landslide hazard under mean rainfall conditions for a specific region before urban development is carried out.

SHIA_Landslide can be a useful framework for investigating how a catchment system would likely respond in the short and long term to a rainfall perturbation from its current state. This advantage permits the user to evaluate the responses of tropical residual soil slopes under rainfall conditions. Knowledge of the processes that govern slope stability conditions and evolution could help in arranging proper tools for hazard analysis and risk management.

The model outputs four useful products during the simulation process. The hydrological module gives the hydrograph and perched water table variation for any point in the catchment. The geotechnical module outputs two maps, a susceptibility map before the target area is exposed to rainfall and a landslide hazard map showing the spatial distribution of landslides triggered by rainfall. The program saves the outputs to a series of ASCII text files that can be imported to GIS software for display or further analysis.

Most physically based models that show high levels of prediction also overestimate landslide occurrence. Compared to SHALSTAB, SHIA_Landslide shows much better performance for the La Arenosa catchment in terms of correctly classified unstable grid cells (hit rate), with similar values for false alarm rate, precision and specificity. Nevertheless, the SHIA_Landslide results also show that more cells are predicted to be unstable than are observed. Clearly, the lack of a complete landslide database for the entire catchment may be (at least partially) responsible for hazard overestimation when simulated and actual scars are compared. However, local effects are not included in the infinite slope model, which, coupled with the uncertainty of some of the model parameters, may generate significant uncertainty in the model results.

The overestimation of landslides could be due to the elimination of other factors influencing landslide occurrence such as vegetation, detailed geological setting and artificial or man-made structures. This study neglected the effects of vegetation in the geotechnical component. The stability estimate was therefore conservative because slopes considered unstable could be stable in reality if significant amounts of root cohesion added to the shear strength.

It is important to keep in mind that the spatial and temporal distribution of landslides is a result of the interaction between many complex hydrological and geotechnical parameters. A reliable, accurate landslide forecasting map depends on the proper determination of these parameters' role. Thus, the inclusion or omission of some of these parameters may significantly change the capability of landslide forecasting.

Acknowledgments

The authors wish to thank the Hans Wildsdorf Foundation and the Colombian Association of Petroleum Geologists and Geophysicist (ACGGP) for providing financial support for conducting this research. We also thank the two anonymous reviewers and the Associate Editor for their constructive and useful comments that greatly improved the manuscript.

References

- Aleotti P, Chowdhury R (1999) Landslide hazard assessment: summary review and new perspectives. *Bull Eng Geol Environ* 58:21–44
- Anderson MG, Lloyd DM (1991) Using a combined slope hydrology-stability model to develop cut slope design charts. *Proc Inst Civ Eng* 91:705–718
- Anderson A, Sitar N (1995) Analysis of rainfall-induced debris flows. *J Geotech Eng* 121:544–552
- Anon (1995) The description and classification of weathered rocks for engineering purposes. Geological Society Engineering Group Working Party Report. *Q J Eng Geol* 28:207–242
- Apip, Takara K, Yamashiki Y, Ibrahim AB, Sassa K, Fukuoka H (2010) A distributed hydrological-geotechnical model using satellite-derived rainfall for shallow landslide warning in a large basin. *Landslides* 7(3):237–258

- Arnaud P, Lavabre J (1995) Couplage de modèles de simulation de hyéogrammes aux pas de temps journalier et horaire. Les modèles au Cemagref - Séminaire inter-rechercheurs (1) - 23–31
- Arnone E, Noto LV, Lepore C, Bras RL (2011) Physically-based and distributed approach to analyze rainfall-triggered landslides at watershed scale. *Geomorphology* 133:121–131
- Askarinejad A, Laue J, Zweidler A, Iten M, Bleiker E, Buschor H, Springman S M (2012) Physical modelling of rainfall induced landslides under controlled climatic conditions. In: Eurofuge 2012, Delft, Netherlands, published on CD only
- Baum R L, Savage W Z, Godt W (2002) TRIGRS—a Fortran program for transient rainfall infiltration and grid-based regional slope-stability analysis. U.S. Geological Survey Open-File Report, 2008-1159, 75 p
- Bergström S (1995) The HBV model. In: Singh VP (ed) Computer models of watershed hydrology. Water Resources Publications, Colorado
- Bertoldi G, Rigon R (2004) Geotop: a hydrological balance model: technical description and programs guide, version 0.875, Technical Report DICA-04-001, University of Trento, Italy
- Biondi D, Freni G, Iacobellis V, Mascaro G, Montanari A (2012) Validation of hydrological models: conceptual basis, methodological approaches and a proposal for a code of practice. *Phys Chem Earth* 42–44:710–776
- Bishop AW (1955) The use of the slip circle in the stability analysis of slopes. *Geotechnique* 5:7–17
- Borga M, Dalla Fontana G, Daros D, Marchi L (1998) Shallow landslide hazard assessment using a physically based model and digital elevation data. *Environ Geol* 35(2–3):81–88
- Brand EW (1985) Predicting the performance of residual soil slopes. *Proc 11th Int Conf Soil Mech Found Eng* 5:2541–2578
- Bray DL (1979) Estimating average velocity in gravel-bed rivers. *J Hydraul Div ASCE* 105:1103–1122
- Brunsdon D (2002) The fifth Glossop Lecture. Geomorphological roulette for engineers and planners: some insights into an old game. *Q J Eng Geol* 35:101–142
- Burton A, Bathurst JC (1998) Physically based modeling of shallow landslide sediment yield at a catchment scale. *Environ Geol* 35(2–3):89–99
- Carrara A, Crosta G, Frattini P (2008) Comparing models of debris-flow susceptibility in the alpine environment. *Geomorphology* 94:353–378
- Cepeda J, Hoeg K, Nadim F (2010) Landslide triggering rainfall thresholds: a conceptual framework. *Q J Eng Geol Hydrogeol* 43:69–84
- Chacón J, Irigaray C, Fernandez T, El Hamdouni R (2006) Engineering geology maps: landslides and geographical information systems. *Eng Geol Environ* 65:341–411
- Collins BD, Znidarcic D (2004) Stability analyses of rainfall induced landslides. *J Geotech Geoenviron* 130(4):362–371
- Corominas J, Moya J (1999) Reconstructing recent landslide activity in relation to rainfall in the Llobregat river basin, Eastern Pyrenees, Spain. *Geomorphology* 30:79–93
- Crosta G (1998) Regionalization of rainfall threshold: an aid for landslide susceptibility zonation. *Environ Geol* 35(2–3):131–145
- Crosta G, Frattini P (2003) Distributed modeling of shallow landslides triggered by intense rainfall. *Nat Hazard Earth Syst Sci* 3:81–93
- Crosta G, Frattini P (2008) Rainfall-induced landslides and debris flows. *Hydrol Process* 22:473–477
- Deere D U, Patton F D (1971) Slope stability in residual soils. En Proc., Fourth Pan American Conference on Soil Mechanics and Foundation Engineering, Puerto Rico. 1:87–170
- Dhakal AS, Sidle RC (2003) Distributed simulations of landslides for different rainfall conditions. *Hydrol Process* 18:757–776
- D'Odorico P, Fagherazzi S (2003) A probabilistic model of rainfall-triggered shallow landslides in hollows: a long term analysis. *Water Resour Res* 39(9):1262
- D'Odorico P, Fagherazzi S, Rigon R (2005) Potential for landsliding: dependence on hyetograph characteristics. *J Geophys Res* 110:1–10
- Edijatno N, Michel C (1989) Un modèle pluie-débit à trois paramètres. *La Houille Blanche* 2:113–121
- Fawcett T (2006) An introduction to ROC analysis. *Pattern Recogn Lett* 27:861–874
- Fell R, Corominas J, Bonnard C, Cascini L, Leroi E, Savage W Z, (2008) Guidelines for landslide susceptibility, hazard and risk zoning for land use planning. *Eng Geol* 102:85–98
- Frances F, Vélez J J, Munera J C, Medici C, Busi G (2012) Descripción del modelo conceptual distribuido de simulación hidrológica TETIS v.8. Universidad Politécnica de Valencia, pp 86
- Frances F, Vélez JJ, Vélez JJ (2007) Split-parameter structure for the automatic calibration of distributed hydrological models. *J Hydrol* 332:226–240
- Frattini P, Crosta G, Fusì N, Dal Negro P (2004) Shallow landslides in pyroclastic soils: a distributed modeling approach for hazard assessment. *Eng Geol* 73:277–295
- Fredlund DG, Rahardjo H (1993) Soil mechanics for unsaturated soils. Wiley, New York, p 517
- Godt JW, Sener-Kaya B, Lu N, Baum RL (2012) Stability of infinite slopes under transient partially saturated seepage conditions. *Water Resour Res* 48:1–14
- Graham J (1984) Methods of stability analysis. In: Brunsden D, Prior DB (eds) Slope instability. Wiley, New York, pp 171–215
- Griffiths J A, Collison A J C (1999) The validity of using a simplified distributed hydrological model for estimation of landslide probability under a climate change scenario. Proceedings of the Fourth International Conference on GeoComputation, Virginia, USA. (<http://www.geocomputation.org/1999/index.html>). Accessed 12 Oct 2012
- Hack JT (1957) Studies of longitudinal stream profiles in Virginia and Maryland. US Geol Surv Prof Pap 294-B:45–97
- Hammond C, Hall D, Miller S, Swetlik P (1992) Level I stability analysis (LISA) documentation for version 2.0, general technical report INT-285, USDA Forest Service Intermountain Research Station
- Hermelin M, Mejía O, Velásquez E (1992) Erosional and depositional features produced by a convulsive event, San Carlos, Colombia, September 21, 1990. *Bull Int Assoc Eng Geol* 45:89–95
- Hey RD (1979) Dynamic process-response model of river channel development. *Earth Surf Process* 4:59–72
- Hutchinson J, Bhandari R (1971) Undrained loading, a fundamental mechanism of mudflows and other mass movements. *Geotechnique* 21(4):353–358
- IGAC – Instituto Geográfico Agustín Codazzi (2007) Estudio general de suelos y zonificación de tierras del departamento de Antioquia. Bogotá, pp 207
- Iida T (1999) A stochastic hydro-geomorphological model for shallow landsliding due to rainstorm. *Catena* 34:293–313
- INTEGRAL S A (1990) Informe sobre daños en la central de calderas por la avalancha ocurrida en la quebrada La Arenosa el 21 de septiembre de 1990 y su reparación. Report Interconexión Eléctrica S.A. ISA. pp 45
- Ivanov VY, Vivoni E, Bras RL, Entekhabi D (2004) Catchment hydrologic response with a fully-distributed triangulated irregular network model. *Water Resour Res* 40:W11102
- Iverson R (2000) Landslide triggering by rain infiltration. *Water Resour Res* 36(7):1897–1910
- Jaramillo A (2006) Evapotranspiración de referencia en la región Andina de Colombia. *Cenicafé* 57(4):288–298
- Klemes V (1986) Operational testing of hydrological simulation models. *Hydrol Sci J* 31:13–24
- Kojima T, Takara K (2003) A grid-cell based distributed flood runoff model and its performance. In: Tachikawa Y, Vieux BE, Georgakakos KP, Nakakita E (eds) Weather radar information and distributed hydrological modelling. IAHS, Publication No. 282, 234–240
- Kubota J, Sivapalan M (1995) Towards a catchment-scale model of subsurface runoff generation based on synthesis of small-scale process-based modeling and field studies. In: Sivapalan M (ed) Scale issues in hydrological modeling. Wiley, New York, pp 297–310
- Larsen MC (2008) Rainfall-triggered landslides, anthropogenic hazards and mitigation strategies. *Adv Geosci* 14:147–153
- Leopold L B, Maddock T J (1953) Hydraulic geometry of stream channels and some physiographic implications. U. S. Geological Survey Professional Paper 252, pp 55
- Leopold L B, Wolman M G, Miller J P (1964) Fluvial Processes and Geomorphology. Freeman and Co., San Francisco, California. pp 522
- Limerinos J T (1969) Relation of the Manning coefficient to measure bed roughness in stable natural channels. U S Geological Survey Professional paper 650D, pp 45
- Little A L (1969) The engineering classification of residual tropical soils. Proceedings of 7th International Conference of Soil Mechanics and Foundation Engineering 1:1–10
- Martínez C (2012) Susceptibilidad a la ocurrencia de movimientos en masa superficiales detonados por lluvia utilizando el modelo SHALSTAB: Cuenca La Arenosa, municipio de San Carlos, Antioquia. Dissertation. University of Antioquia, Medellín, pp 60
- Mejía R, Velásquez M E (1991) Procesos y depósitos asociados al aguacero de septiembre 21 de 1990 en el Área de San Carlos (Antioquia). Dissertation, University of Colombia, Medellín, pp 160
- Montgomery DR, Dietrich WE (1994) A physically based model for the topographic control of shallow landsliding. *Water Resour Research* 30:1153–1171
- NOAA—National Oceanic and Atmospheric Administration, USGS—United States Geological Survey (2005) NOAA-USGS debris flow warning system. Final report, circular 1283. <http://pubs.usgs.gov/circ/2005/1283/>. Accessed 11 January 2012
- O'Loughlin EM (1986) Prediction of surface saturation zones in natural catchments by topographic analysis. *Water Resour Res* 22:794–804

- Pack R T, Tarboton D G, Goodwin C N (1998) Terrain stability mapping with SINMAP, technical description and users guide for version 1.00, Report Number 4114-0, Terratech Consulting Ltd, Salmon Arm, BC, Canada
- Paniconi C, Troch PA, van Loon EE, Arno G, Hilberts J (2003) Hillslope-storage Boussinesq model for subsurface flow and variable source areas along complex hillslopes: 2. Intercomparison with a three-dimensional Richards's equation model. *Water Resour Res* 39(11):1317–1329
- Parsons AJ, Abrahams AD, Wainwright J (1994) On determining resistance to interrill overland flow. *Water Resour Res* 30(12):3515–3521
- Rahardjo H, Leong EC, Rezaur RB (2008) Effect of antecedent rainfall on pore-water pressure distribution characteristics in residual soil slopes under tropical rainfall. *Hydrol Process* 22:506–523
- Rahardjo H, Li XW, Toll DG, Leong EC (2001) The effect of antecedent rainfall on slope stability. *Geotech Geoenviron Eng* 19:371–399
- Rahardjo H, Lim TT, Chang MF, Fredlund DG (1995) Shear strength characteristics of a residual soil. *Can Geotech J* 32:60–77
- Restrepo P, Jorgensen D P, Cannon S H, Laber J E, Major J, Marter J A, Purpura J, Werner K (2008) Prototype debris flow warning system for recently burned areas in Southern California. *Bulletin of the Meteorological Society, Insights and Innovation, American Meteorological Society*, pp 1845–1851
- Rezzoug A, Schumann A, Chiffillard P, Zepp H (2005) Field measurements of soil moisture dynamics and numerical simulation using the kinematic wave approximation. *Adv Water Resour* 28:917–926
- Richards LA, Weaver LR (1944) Moisture retention by some irrigated soils as related to soil moisture tension. *J Agric Res* 69:215–235
- Rossi G, Catani F, Leoni L, Segoni S, Tofani V (2013) HIRESSS: a physically based slope stability simulator for HPC applications. *Nat Hazards Earth Syst Sci* 13(13) 151–166
- Sassa K, Wang, G H (2005) Mechanism of landslide-triggered debris flows: liquefaction phenomena due to the undrained loading of torrent deposits. *Debris-flow hazards and related phenomena*. Springer Praxis Books 81–104
- Saxton KE, Rawls WJ (2006) Soil water characteristic estimates by texture and organic matter for hydrologic solutions. *Soil Sci Soc Am J* 70:1569–1578
- Schuster RL (1996) Socioeconomic significance of landslides. In: Turner AK, Schuster RL (eds) *Landslides investigation and mitigation*. Transportation Research Board, National Research Council, Special Report 247. National Academy Press, Washington, pp 129–177
- Sidle RC, Ochiai H (2006) Landslides: processes, prediction, and land use. *Water Resources Monograph 1*. American Geophysical Union, Washington
- Simoni S, Zanotti F, Bertoldi G, Rigon R (2008) Modelling the probability of occurrence of shallow landslides and channelized debris flows using GEOTop-FS. *Hydrol Process* 22:532–545
- Singh VP (2003) On the theories of hydraulic geometry. *Int J Sediment Res* 18(3):196–218
- Singh V P, Dickinson W T (1975) An analytical method to determine daily soil moisture. *Proceedings of the Second World Congress on Water Resources*, Delhi, India (4): 355–365
- Strickler A (1923) Beiträge zur Frage des Geschwindigkeitsformel und der Rauhigkeitszahlen für Strome, Kanale und Geschlossene Leitungen. *Mitteilungen des Eidgenössischer Amtes für Wasserwirtschaft*, Bern, Switzerland
- Takasao T, Shiiba M (1988) Incorporation of the effect of concentration of flow into the kinematic wave equations and its applications to runoff system lumping. *J Hydrol* 102:301–322
- Take WA, Bolton MD, Wong PCP, Yeung FJ (2004) Evaluation of landslide triggering mechanisms in model fill slopes. *Landslides* 1:173–184
- Terlien MTJ (1998) The determination of statistical and deterministic hydrological landslide-triggering thresholds. *Environ Geol* 35(2–3):124–130
- Troch P, van Loon E, Hilberts A (2002) Analytical solutions to a hillslope-storage kinematic wave equation for subsurface flow. *Adv Water Resour* 25:637–649
- Veihmeyer FJ, Hendrickson AH (1928) Plants. *Plant Physiol* 3(3):355–357
- Vélez J I (2001) Desarrollo de un modelo hidrológico conceptual distribuido orientado a la simulación de crecidas. Valencia. Dissertation. Universidad Politécnica de Valencia, pp 202
- Vélez JI, Villarraga MR, Álvarez OD, Alarcón JE, Quintero F (2004) Modelo distribuido para determinar la amenaza de deslizamiento superficial por efecto de tormentas intensas y sismos. XXI Congreso latinoamericano de hidráulica, São Pedro, Brasil, p 8
- Wang G, Sassa K (2003) Pore pressure generation and movement of rainfall-induced landslides: effects of grain size and fine particle content. *Eng Geol* 69:109–125
- Wu W, Sidle R C (1995) A distributed slope stability model for steep forested basins. *Water Resour*

E. Aristizábal (✉)

Environmental Department,
ISAGEN S.A. E.S.P.,
Medellín, Colombia
e-mail: evaristizabal@isagen.com.co

J. I. Vélez

Geoscience School,
National University of Colombia,
Medellín, Colombia

J. Vélez

e-mail: jivelez@unal.edu.co

H. E. Martínez

Civil Engineering Department,
Brasília University,
Brasília, Brazil
e-mail: carvajal@unb.br

M. Jaboyedoff

Centre de recherché sur l'Environnement Terrestre,
University of Lausanne,
Lausanne, Switzerland
e-mail: michel.jaboyedoff@unil.ch